Available online at www.sciencedirect.com
ScienceDirect
Trans. Nonferrous Met. Soc. China 35(2025) 3595−3616
Transactions of Nonferrous Metals Society of China
www.tnmsc.cn

Castability, mechanical, and corrosion properties of Al−Zn−Ca alloys with high thermal conductivity

A. A. LYSKOVICH[1], V. E. BAZHENOV[1], I. I. BARANOV[1], V. A. BAUTIN[2], A. V. SANNIKOV[1], A. I. BAZLOV[3], E. I. TIAN[1], A. A. STEPASHKIN[4], A. V. KOLTYGIN[1], V. D. BELOV[1]

1. Casting Department, National University of Science and Technology “MISIS”, Moscow 119049, Russia;
2. Department of Metallurgy Steel, New Production Technologies and Protection of Metals, National University of Science and Technology “MISIS”, Moscow 119049, Russia;
3. Laboratory of Advanced Green Materials, National University of Science and Technology “MISIS”, Moscow 119049, Russia;
4. Center of Composite Materials, National University of Science and Technology “MISIS”, Moscow 119049, Russia

Received 14 March 2024; accepted 13 November 2024

Abstract: The majority of industrial aluminum casting alloys exhibit low thermal conductivity, which is insufficient for effective heat transfer in electronic devices. The objective of this investigation was to develop new aluminum casting alloys with high thermal conductivity. The impact of alloying elements on the thermal conductivity of pure aluminum was examined, and the relationships among microstructure, thermal conductivity, and the mechanical and corrosion properties of Al−Zn−Ca−(Cu,Mg) alloys were explored. The findings indicate that in the as-cast state, the structure of the alloys consists of α-Al and a eutectic containing the $(Al,Zn)_4Ca$ phase. Following the solution heat treatment, the $(Al,Zn)_4Ca$ phase is spheroidised, and thermal conductivity of the alloys increases, reaching over 75% that of pure aluminum. However, the heat-treated alloys exhibit low mechanical properties: tensile yield strength <60 MPa, ultimate tensile strength <160 MPa, and elongation at fracture >15%. The alloys demonstrate satisfactory fluidity and low hot tearing susceptibility. With the exception of the alloy containing copper, the alloys exhibit low corrosion rates, estimated at approximately 0.02 mm/a.

Key words: aluminum alloys; thermal conductivity; phase composition; fluidity; hot tearing susceptibility; corrosion rate

1 Introduction

Aluminum alloys are widely used in electronics and mechanical engineering due to the unique combination of performance properties: low density, good tensile strength, and high corrosion resistance [1,2]. However, there is currently a need for high thermal conductivity alloys to ensure efficient heat removal from electric vehicle batteries and LED panels. Aluminum alloys with high thermal conductivity are promising candidates for producing parts that require heat transition or dissipation.

Currently, most aluminum alloys with high thermal conductivity are wrought alloys, which limits the geometry of future products [3]. As a result, heat sinks for LED lights are often produced by die casting due to the large number of thin fins [4−6]. The Al−Si alloys are the most commonly used aluminum alloys for die casting. However, alloys like ADC12, which have excellent castability

Corresponding author: V. E. BAZHENOV, E-mail: V.E.Bagenov@gmail.com
https://doi.org/10.1016/S1003-6326(25)66901-9
1003-6326/© 2025 The Nonferrous Metals Society of China. Published by Elsevier Ltd & Science Press
This is an open access article under the CC BY-NC-ND license (http://creativecommons.org/licenses/by-nc-nd/4.0/)

and mechanical properties, exhibit very low thermal conductivity, approximately half that of pure aluminum. The primary reason for the low thermal conductivity of casting alloys is the significant amount of dissolved alloying elements in α-Al, which hinders the free movement of electrons and phonons [7−10]. Additionally, the thermal conductivity of aluminum alloys is affected by the type and fraction of the second phases [11]. For instance, in Al−Si alloys, Si has low solubility, which only slightly distorts the Al lattice [12]. However, even in binary Al–Si alloys, Si significantly reduces the thermal conductivity of aluminum [13]. Therefore, searching for new alloying systems for development of a highly thermally conductive casting alloys is important.

A reasonable choice of alloy composition is the key to developing a new aluminum alloy with high thermal conductivity and good castability. Therefore, studying the influence of alloying elements on the thermal conductivity of aluminum alloys is needed. Previous studies have shown how certain elements such as Si, Mg, Cu, Zn, Cr, V, Mn, Fe, Ti and Zr can affect the thermal conductivity of aluminum alloys [13,14]. The development of a highly thermally conductive casting alloy relies heavily on the use of a eutectic-forming element that is practically insoluble in aluminum [15−18]. However, the influence of many eutectic-forming metals on thermal conductivity remains unclear.

In this work, 14 groups of binary alloys were investigated, including Al−Mg, Al−Ca, Al−Ti, Al−Mn, Al−Cu, Al−Zn, Al−Y, Al−Zr, Al−Si, Al−La, Al−Gd, Al−Cr, Al−Ni, and Al−Fe. The elements selected for this study can be divided into two categories: (1) those with significant maximum solid solubility in α-Al, such as Mg, Ti, Mn, Cu, Zn, Si, Zr, and Cr; (2) those with negligible solubility in α-Al, such as Ca, Y, Gd, La, Ni, and Fe.

The Al−Ca system is a promising alternative to Al−Si for achieving high castability due to its short freezing range and high volume fractions of eutectic [19,20]. Previous studies [13,14] have shown that Zn, Cu and Mg have a less negative impact on the thermal conductivity of aluminum. Moreover, these elements are known to have a strengthening effect on α-Al [21−23]. In addition, alloys of the Al−Ca−Zn system are capable of superplasticity and have high corrosion resistance [24−26]. At the same time, alloys with eutectic Al_4Ca phase can demonstrate good mechanical properties. For example, alloys with the composition Al−(3−4)Ca−(9−11)Zn−3.5Mg(wt.%) demonstrated a hardness of at least HB 200 after aging [27,28]. Therefore, the Al−Zn−Ca alloy system was chosen for study.

The objective of this study is to investigate new promising Al−Zn−Ca aluminum alloys that combine high thermal conductivity with good castability. A comprehensive investigation was conducted to elucidate the relationship among microstructure, thermal conductivity, mechanical and corrosion properties in both the cast and heat-treated states.

2 Experimental

To choose the alloys for investigation, the phase compositions and the freezing ranges of the Al−Zn−Ca−X alloys (X=Cu and Mg) were calculated using Thermo-Calc Software [29] with version 4 of the TCAl4 aluminum-based alloy database [30]. The solidus temperatures of binary Al alloys were also calculated via Thermo-Calc software.

In order to determine the effect of different alloying elements on the thermal conductivity of Al, ingots (100 g) of aluminum-based binary alloys with Mg, Ca, Ti, Mn, Cu, Zn, Y, Zr, Si, La, Gd, Cr, Ni and Fe were prepared. The alloys were melted in a clay−graphite crucible using a high-frequency induction furnace. Prepared melt was poured into the steel mold preheated to 150 °C.

The following high purity raw materials were used for the preparation of alloys: Al (99.99 wt.%), Zn (99.98 wt.%), Mg (99.95 wt.%), Cu (99.96 wt.%), and La (99.8 wt.%). Also, the following master alloys were used: Al−8wt.%Ca, Al−11wt.%Mn, Al−5wt.%Ti, Al−12wt.%Y, Al−5wt.%Zr, Al−13wt.%Gd, Al−10wt.%Cr, Al−4wt.%Ni, and Al−10wt.%Fe. The master alloys were prepared by melting in a clay−graphite crucible using a high-frequency induction furnace.

To facilitate the maximal dissolution of the alloying elements in the aluminum solid solution (α-Al), solid solution heat treatment (SSHT) was conducted for 100 h at 20−50 °C lower than the solidus temperature of the alloys calculated via Thermo-Calc software. Subsequently, the samples

were sectioned from the ingots and ground. The electrical conductivity was measured using an eddy current conductivity meter VE−27NC "Sigma" with a measurement range of 5.0−37.0 MS/m, and the thermal conductivity was calculated. In addition, the metallographic sections were prepared, and the element contents in α-Al were measured by energy-dispersive X-ray spectroscopy (EDS).

The thermal conductivity (λ) was calculated from the electrical conductivity (σ) measurements using the linear empirical relationship as [31,32]

$$\lambda=AL_0T\sigma+B \quad (1)$$

where L_0 is the Lorenz number (2.45×10^{-8} W·Ω·K^{-2} [31]), T is the thermodynamic temperature, and A and B are empirical constants.

Figure 1 shows the relationship between the thermal conductivity and electrical conductivity of aluminum alloys. The linear relationship (blue line) is obtained from the thermal and electrical conductivity data for 140 wrought and casting commercial aluminum alloys and pure Al from previous reports [33]. The linear relationship between thermal conductivity and electrical conductivity reported by ZHENG et al [31] (A and B was 0.909 and 10.5 W/(m·K), respectively) is close to those found, especially for alloys with low thermal conductivity. The following equation was obtained:

$$\lambda=0.816L_0T\sigma+17.94 \quad (2)$$

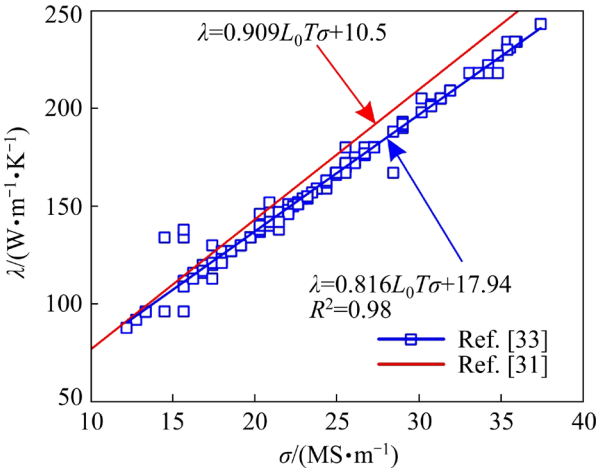

Fig. 1 Linear relationship between thermal and electrical conductivities of commercial aluminum alloys

Seven Al−Zn−Ca−X alloys, where X=Cu and Mg, were prepared by melting in a clay−graphite crucible using an induction furnace. The charge for each alloy was 5 kg. Prior to casting, the melt was degassed with hexachloroethane and held for 10 min. The pouring temperature of the probes and samples used for further investigations was 720 °C. The heat treatment was performed based on the T4 heat-treatment mode, consisting of a SSHT at 500 °C for 5 h and 550 °C for 5 h followed by quenching in water.

The microstructures of the alloys and the compositions of the phases were investigated using energy-dispersive X-ray spectroscopy (EDS) on a Tescan Vega SBH3 scanning electron microscope with an Oxford EDS detector. The as-cast and heat-treated alloy samples were ground and polished for metallographic observations. The chemical compositions of the prepared alloys were determined using EDS on three areas with dimensions of 1 mm × 1 mm and presented in Table 1.

Table 1 Chemical compositions of alloy samples (wt.%)

Sample No.	Designation	Zn	Ca	Cu	Mg	Al
1	AlZn1Ca2	1.1	2.1	−	−	Bal.
2	AlZn3Ca2	3.1	2.1	−	−	Bal.
3	AlZn5Ca2	5.1	2.0	−	−	Bal.
4	AlZn3Ca3	3.2	3.2	−	−	Bal.
5	AlZn3Ca4	3.1	4.2	−	−	Bal.
6	AlZn3Ca2Cu1	3.1	2.0	1.0	−	Bal.
7	AlZn3Ca2Mg1	3.0	1.9	−	1.1	Bal.

The alloy phase compositions in the as-cast state were studied via X-ray diffractometry (XRD) with a Bruker D8 ADVANCE (Karlsruhe, Germany) diffractometer under monochromatic Cu K_α radiation on powder alloy samples.

The fluidity of the alloys was determined using spiral probe at a melt pouring temperature of 720 °C. For testing, green sand molds were made. The fluidity of each alloy was the average length of the spiral probe. Three spiral probe castings were made for each alloy. The probe and mould dimensions, and test scheme can be found elsewhere [34]. Hot tearing resistance was determined using the dog-bone test [18]. The measure of hot tearing resistance is hot tearing criterion that is the maximum length of the branch without cracks. The higher hot tearing criterion corresponds to higher hot tearing resistance. The maximum length of the branch that can be obtained

using this probe is 80 mm. Three probes for each alloy were poured.

In order to approve the thermal conductivity measurements based on electrical conductivity, another method of thermal conductivity determining was used for one of the alloys. The relationship of temperature, density (ρ), thermal diffusivity (a), and specific heat capacity (C_p) was characterized using third-order polynomials. Thermal conductivity (λ) was determined using Eq. (3):

$$\lambda=a\rho C_p \quad (3)$$

Density at room temperature (25 °C) was measured using hydrostatic weighing. The variation of density with temperature was derived through the thermal expansion coefficient, which was ascertained using a NETZSCH DIL 402 C (Germany) dilatometer (DIL). The laser flash method (LFA) was used to measure the thermal diffusivity with the NETZSCH LFA 447 (Germany). The temperature dependence of specific heat capacity of aluminum was calculated using NIST JANAF equations [35].

For tensile mechanical test, the ingots with dimensions of 32 mm × 340 mm × 50 mm were poured into a graphite mold [18]. After that, cylindrical tensile samples with gauge diameter and length of 5 and 50 mm respectively were machined from the resulting ingot. Tensile tests were carried out on an Instron 5569 (USA) universal testing machine with advanced video extensometer (AVE).

To assess the hardness and electrical conductivity for each alloy, the cylindrical ingots with diameter of 35 mm and length of 150 mm were cast into a steel mold. Further, discs with 10 mm in height were cut out from the central part of the ingot by a band-saw. To measure the hardness and electrical conductivity, one of the surfaces of each disc was ground. After the samples were subjected to heat treatment, the hardness and electrical conductivity were also measured. Brinell hardness was studied on an INNOVATEST Nemesis 9001 (Netherlands) universal hardness tester. Test parameters: indenter (a ball with a diameter of 2.5 mm), load 613 N, and holding time 10 s under load.

Immersion corrosion testing was carried out on rectangular specimens of 15 mm × 15 mm × 15 mm in size (surface area ~13.5 cm^2). For each alloy in as-cast condition and after SSHT, four samples were cut. Next, the samples were ground using 320 grit abrasive SiC paper and weighed on the balance of HR−202i model (AND, Japan). During the immersion test, the samples were immersed in a 400 mL solution of 5.7% NaCl + 0.3% H_2O_2 in distilled water at 25 °C for 15 d [36]. This solution and immersion test procedure is intended to evaluate the development of corrosion in wrought and casting aluminum alloys as a production control test. The peroxide was introduced immediately before the start of the test and was added again every 5 d due to its decomposition in the aqueous environment. Once test was finished, the samples were extracted and dried. The corrosion products were removed by dipping samples into concentrated HNO_3 for 1 min to avoid reactions that may result in excessive removal of base metal [37]. Next, specimens were washed with distilled water. The etching operation was continued until the mass loss of the samples was ±0.001 g. The samples were then re-weighed to determine the mass gain per unit surface area. Finally, the average corrosion rate was calculated according to the ASTM standard [37].

The electrochemical investigations were conducted in a 5.7% NaCl + 0.3% H_2O_2 aqueous solution at 25 °C using the IPC Pro MF potentiostat/galvanostat/FRA with the three-electrode corrosion system. The alloy samples were used as the working electrodes, with an approximate area of ~1.3 cm^2. Platinum and saturated silver/silver chloride (Ag/AgCl) electrodes were used as the counter and reference electrodes, respectively. Before electrochemical analysis, the alloy samples were ground and washed in distilled water. Potentiodynamic polarization tests were performed from cathodic region (at −1.6 V) to anodic region (at −0.4 V) with a scan rate of 1 mV/s. The corrosion current density and corrosion potential were derived through Tafel fitting, and then the corrosion rate was calculated from the data obtained [38].

To evaluate the potential application of the developed alloys, the properties of the Al−Zn−Ca alloys investigated were compared with the widely used commercial A356 aluminum casting alloy prepared in the same manner. The heat treatment followed the T4 heat-treatment mode, which involved a SSHT at 535 °C for 5 h followed by quenching in water.

3 Results

3.1 Effect of Mg, Ca, Ti, Mn, Cu, Zn, Y, Zr, Si, La, Gd, Cr, Ni and Fe on thermal conductivity of Al

For choosing the alloying elements and their maximal concentration in developed alloy, the effect of Mg, Ca, Ti, Mn, Cu, Zn, Y, Zr, Si, La, Gd, Cr, Ni and Fe on thermal conductivity of Al was studied. Figure 2 shows the dependence of thermal conductivity (λ), calculated by measured electrical conductivity using Eq. (2), for different binary aluminum alloys containing Mg, Ca, Ti, Mn, Cu, Zn, Y, Zr, Si, La, Gd, Cr, Ni and Fe, and their content in α-Al (Table 2). Figure 2(a) shows the thermal conductivity of binary alloys with meaningful solubility of elements in α-Al. The results show that Zn exhibits the smallest reduction in thermal conductivity of Al. The thermal conductivity of the alloy with 10 wt.% Zn decreases from 235 to ~180 W/(m·K). Therefore, Zn was chosen as the main alloying element. Mg and Cu reduce thermal conductivity more than Zn, but when their content is up to 1 wt.%, the thermal conductivity of binary alloys is ~213 W/(m·K). Hence, it is possible to use Mg and Cu but only in small amount. Ti, Cr, Zr, Si and Mn greatly decrease the thermal conductivity of Al, even at low levels. As regards elements with low solubility in the solid α-Al, RE only slightly reduces the thermal conductivity of Al (Fig. 2(b)). This is due to the fact that the atomic radius of RE differs significantly from Al. RE actively interacts with Al, forming dispersoids of the Al_3RE-type during annealing in the α-Al solid solution. Forming these particles, in turn, can lead to noticeable strengthening of the alloy [39,40]. However, using RE in commercial alloys is challenging due to the high cost. At the same time, the addition of Ca to Al only slightly reduces its thermal conductivity. Notably, the thermal conductivity of the binary alloy with 4 wt.% Ca was about 200 W/(m·K). Binary alloys with Fe and Ni, on the other hand, rapidly reduced the thermal conductivity of Al at low contents. The thermal conductivity of the binary alloys confirms that the Al−Zn−Ca−(Cu,Mg) system is promising for developing an alloy that exhibits high thermal conductivity.

3.2 Phase composition of Al−Zn−Ca−(Cu,Mg) alloys

Figure 3 shows the polythermal sections of the Al−Zn−Ca−(Cu,Mg) phase diagrams that were calculated using the Thermo-Calc program. The liquidus and solidus lines are marked in red and blue, respectively. According to the calculation results, after solidification of the Al−Zn−Ca alloys, the Zn content up to 5 wt.% and Ca content up to 4 wt.%, the following phases are presented: α-Al, Al_4Ca, and $CaZn_{11}$. After alloying the Al−Zn−Ca alloys by Cu or Mg, Al_2Cu or $MgZn_2$ and $Al_2Mg_3Zn_3$ phases may precipitate. With an increase in the content of Zn and Cu, the liquidus temperature remained almost constant. An increase in the amount of Ca and Mg leads to a decrease in the liquidus temperature. Solidus temperatures also decrease as the amount of added alloying elements increases. For example, at 4 wt.% Cu, solidus temperature was 525 °C.

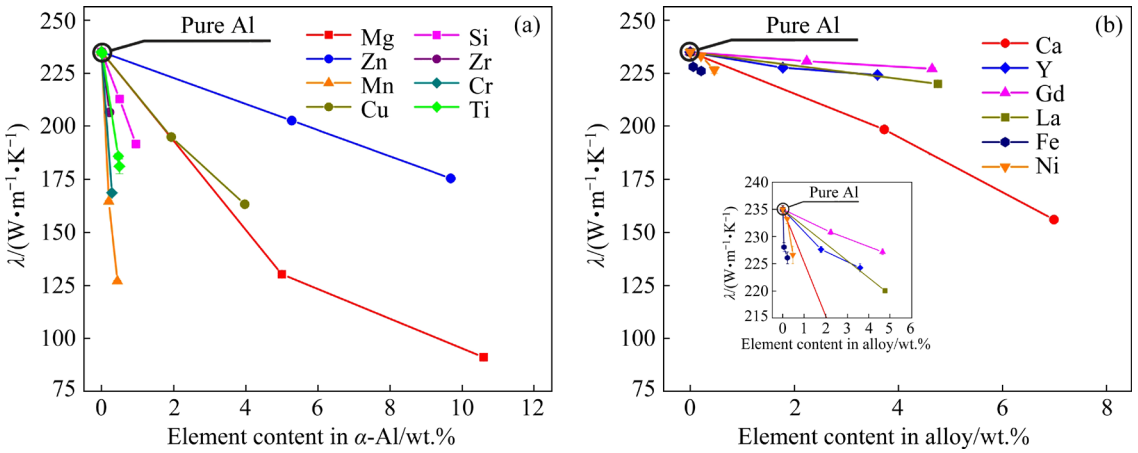

Fig. 2 (a) Effect of element content dissolved in α-Al on thermal conductivity of alloys; (b) Thermal conductivity of binary aluminum alloys with components having negligible solid solubility in α-Al

Table 2 Chemical compositions, electrical conductivity and thermal conductivity of binary aluminum alloy samples at different SSHT temperatures

Element	SSHT temperature/°C	Content/wt.%		Electrical conductivity/ ($MS·m^{-1}$)	Thermal conductivity/ ($W·m^{-1}·K^{-1}$)
		In alloy	In α-Al solid solution		
Mg	450	5.0	5.0	18.9	130.2
	450	10.6	10.6	12.3	91.2
Ca	550	3.7	<0.1	30.3	198.5
	550	7.0	0.5	23.2	156.0
Ti	600	0.3	0.5	28.2	185.9
	600	0.7	0.5	27.4	181.2
Mn	600	0.9	0.4	18.3	127.0
	600	0.4	0.2	24.6	164.6
Cu	500	4.5	4.0	24.4	163.2
	500	2.0	1.9	29.7	195.0
Zn	600	5.5	5.3	31.0	202.7
	600	11.0	9.7	26.4	175.4
Y	600	1.8	<0.1	35.2	227.6
	600	3.6	<0.1	34.6	224.3
Zr	600	0.2	0.2	31.7	206.6
Si	550	0.9	1.0	29.2	191.6
	550	0.5	0.5	32.7	212.8
La	600	4.8	<0.1	33.9	220.1
Gd	600	4.7	<0.1	35.1	227.2
	600	2.2	<0.1	35.7	230.8
Cr	600	0.3	0.3	25.3	168.7
Ni	600	0.1	<0.1	36.1	233.2
	600	0.4	<0.1	35.0	226.6
Fe	600	0.1	<0.1	35.3	228.1
	600	0.6	<0.1	34.9	226.1

Figure 4 shows the solidification pathways calculated using the Sheil−Gulliver model for the alloys presented in Table 1. These alloys were chosen to determine the effect of the alloying element content on the phase composition and the freezing range of the Al−Zn−Ca−(Cu,Mg) alloys under non-equilibrium solidification conditions. It was known that the rapid cooling occurred during alloy solidification in cast parts is better characterized by the Scheil−Gulliver solidification model. All Al−Zn−Ca ternary alloys have an identical solidification pathway. In this regard, solidification pathways shown only for AlZn3Ca2 alloy, and for other alloys are not presented. At the first stage, primary α-Al crystals are formed. Next, Al_4Ca is precipitated according to the eutectic reaction. In the case of Cu alloying, in addition to the binary eutectic reaction $L \rightarrow \alpha\text{-Al}+Al_4Ca$, a ternary eutectic reaction occurs with precipitation of the Al_2Cu phase (Fig. 4(b)). Similar changes occur when alloying with Mg. The alloy with 1 wt.% Mg has the ternary eutectic reaction such as $L \rightarrow \alpha\text{-Al}+Al_4Ca+Al_2Mg_3Zn_3$ (Fig. 4(c)). As a result, alloying with 1 wt.% Cu or 1 wt.% Mg leads to an increase in the non-equilibrium freezing range from 112 °C (AlZn3Ca2) to 161 and 170 °C, respectively.

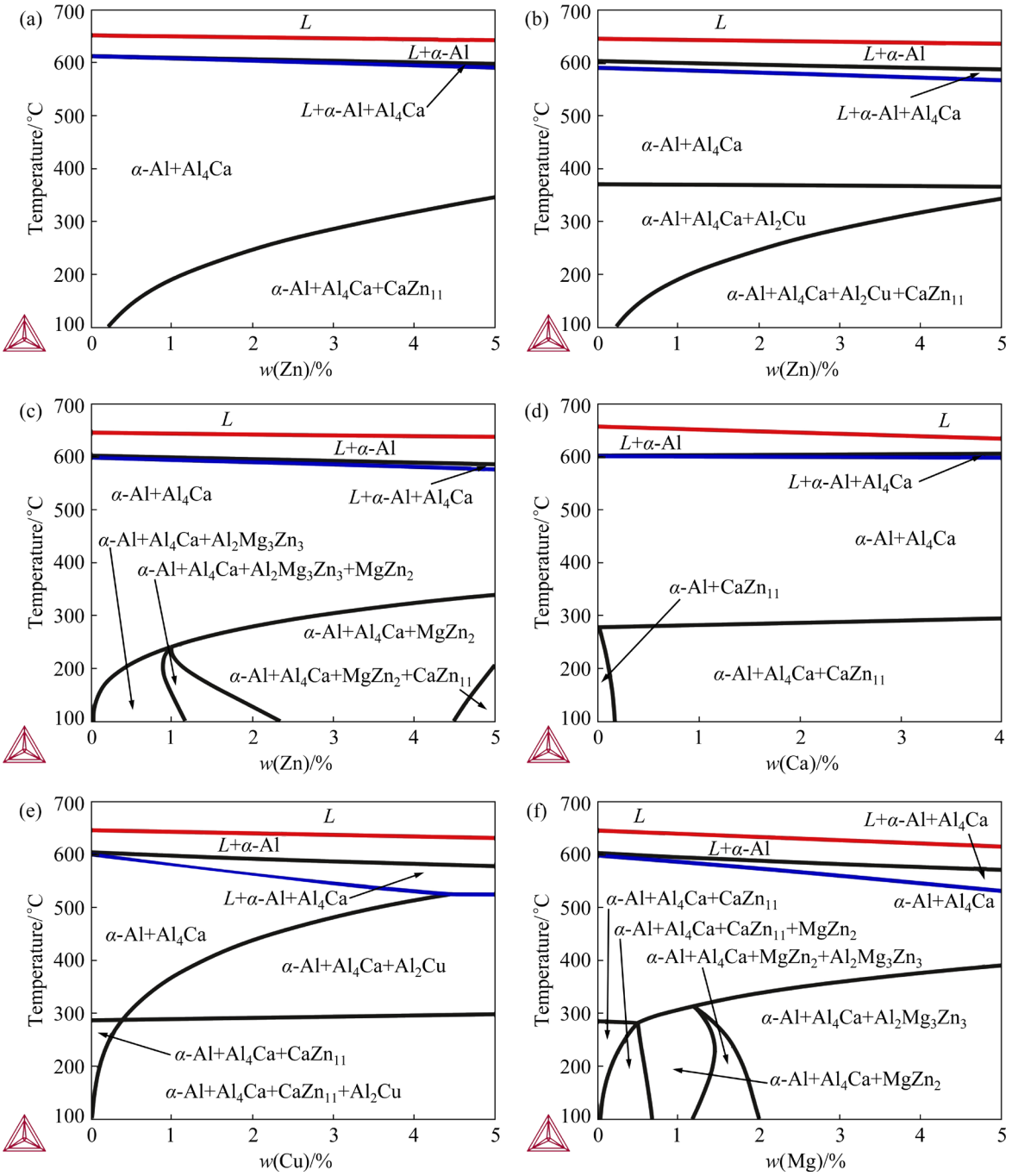

Fig. 3 Polythermal sections of Al−Zn−Ca−(Cu,Mg) phase diagrams: (a) Al−2%Ca−(0−5)%Zn; (b) Al−2%Ca−1%Cu−(0−5)%Zn; (c) Al−2%Ca−1%Mg−(0−5)%Zn; (d) Al−3%Zn−(0−4)%Ca; (e) Al−3%Zn−2%Ca−(0−5)%Cu; (f) Al−3%Zn−2%Ca−(0−5)%Mg

It is well known that a long freezing range is undesirable and may increase the tendency of shrinkage porosity and hot tear formation in the castings [41,42].

3.3 Microstructures of Al−Zn−Ca−(Cu,Mg) alloys

The microstructures of the Al−Zn−Ca−(Cu,Mg) alloys in the as-cast and SSHT conditions are shown in Fig. 5. The microstructure of alloys consists of α-Al primary crystals and α-Al+Al_4Ca eutectic. In the as-cast state, the eutectic had the form of lamellas of Al_4Ca in solid solution α-Al matrix. After heat treatment, the Al_4Ca eutectic was fragmented and spheroidized with subsequent growth of fragments up to ~3.0 μm (AlZn3Ca2). The main difference in structure for the prepared alloys is the eutectic fraction. With an increase in

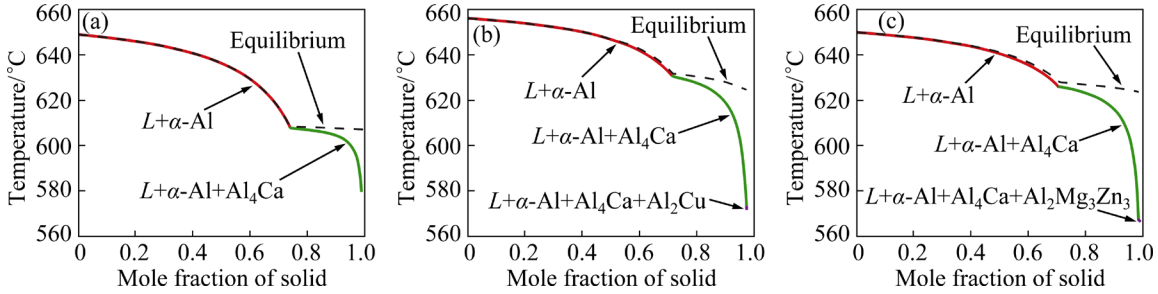

Fig. 4 Scheil−Gulliver model solidification pathway of Al−Zn−Ca−(Cu,Mg) alloys calculated using Thermo-Calc: (a) AlZn3Ca2; (b) AlZn3Ca2Cu1; (c) AlZn3Ca2Mg1

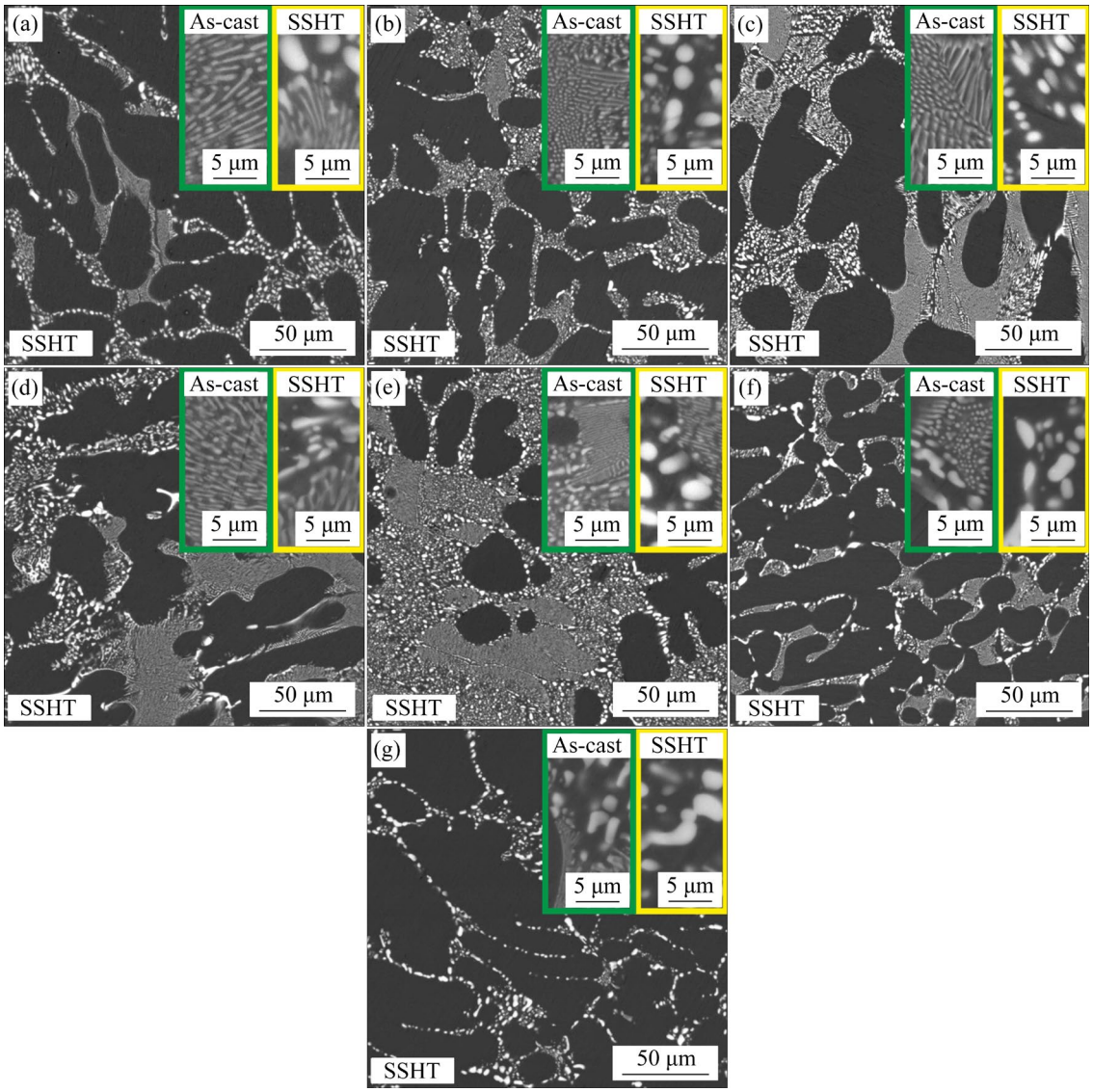

Fig. 5 Microstructures of Al−Zn−Ca−(Cu,Mg) alloys in as-cast and SSHT conditions: (a) AlZn1Ca2; (b) AlZn3Ca2; (c) AlZn5Ca2; (d) AlZn3Ca3; (e) AlZn3Ca4; (f) AlZn3Ca2Cu1; (g) AlZn3Ca2Mg1

the amount of Zn in the as-cast alloys from 1 to 5 wt.%, the fraction of eutectic increases from 23.4 to 29.6 vol.% (Fig. 6(a)). A similar dependence is observed as Ca content increases from 2 to 4 wt.% and the fraction of eutectic in the alloys increases from 25.4 to 59.0 vol.%. The alloying of 1 wt.% Cu or Mg leads to a decrease of the eutectic from 25.4 (AlZn3Ca2) to 22.9 and 15.5 vol.%, respectively.

The data are fully consistent with the EDS analysis results presented in Fig. 7 and Table 3. The findings indicate that the majority of Zn is present in the eutectic, although a portion remains in the α-Al solid solution. Conversely, Ca is concentrated exclusively in the eutectic. This indicates that phases based on it are formed in the alloys. According to Figs. 7(d, h), and Table 3, Mg is evenly dissolved in α-Al and eutectic region, while Cu is concentrated in the eutectic mostly.

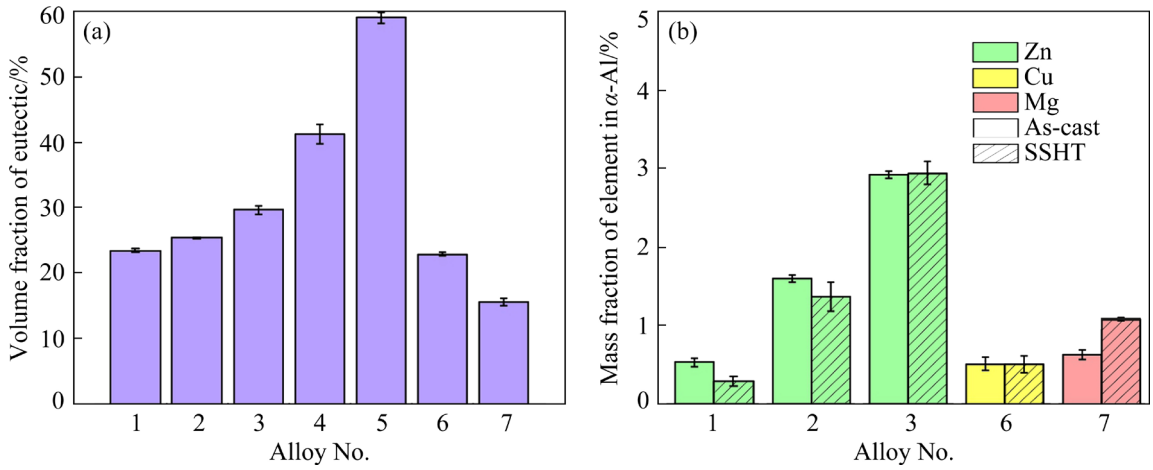

Fig. 6 (a) Volume fraction of eutectic in as-cast alloys; (b) Zn, Cu and Mg contents in α-Al solid solution in as-cast and SSHT states

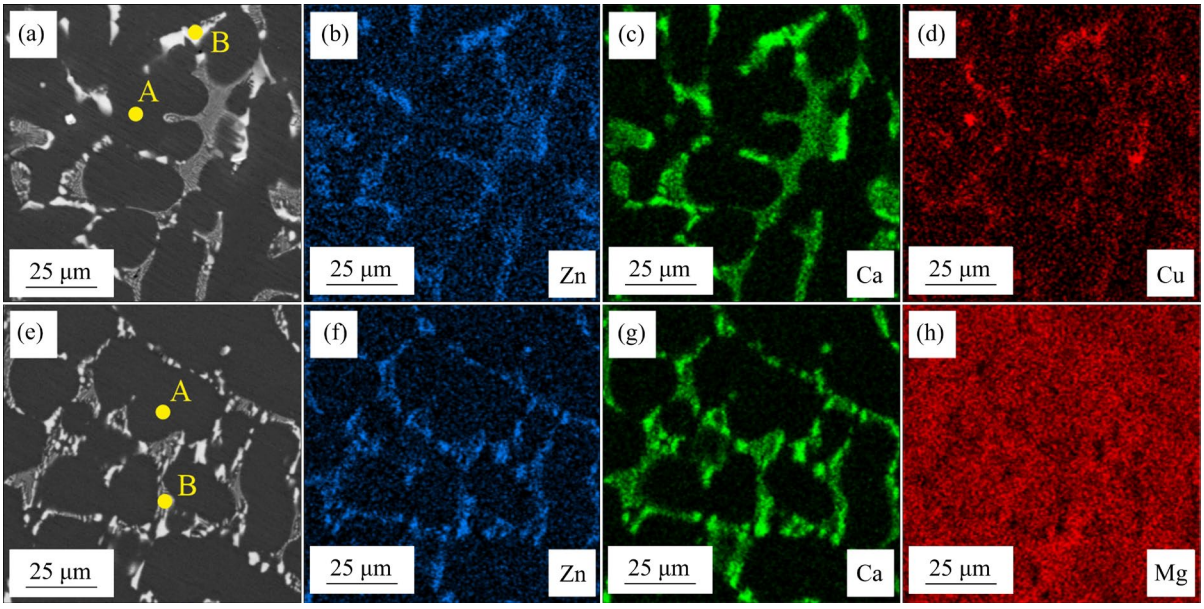

Fig. 7 SEM images of AlZn3Ca2Cu1 (a) and AlZn3Ca2Mg1 (e) alloys in as-cast state, and EDS maps of Zn (b), Ca (c) and Cu (d) in AlZn3Ca2Cu1 alloy and Zn (f), Ca (g) and Mg (h) in AlZn3Ca2Mg1 alloy

Table 3 Average composition of α-Al solid solution (A) and eutectic (B) regions in as-cast alloys determined by EDS

Alloy	Region	Content/at.% (wt.%)				
		Zn	Ca	Cu	Mg	Al
AlZn3Ca2Cu1	A	0.7(1.7)	<0.1(<0.1)	0.2(0.5)	−	Bal.
	B	4.3(9.2)	7.9(10.3)	1.6(3.2)	−	Bal.
AlZn3Ca2Mg1	A	0.6(1.5)	<0.1(<0.1)	−	0.7(0.6)	Bal.
	B	4.7(10.1)	7.4(9.8)	−	1.2(1.0)	Bal.

The elemental composition of the α-Al solid solution of as-cast and heat-treated Al−Zn−Ca−(Cu,Mg) alloys obtained by EDS is shown in Fig. 6(b). With an increase in the Zn content in as-cast alloys from 1 to 5 wt.%, the amount of Zn in α-Al solid solution increased from 0.5 to 2.9 wt.%. This is directly related to the high solubility of Zn in Al. The Ca content is lower than detection limit of EDS analysis. The Cu and Mg contents in α-Al are two times less than the amount of these elements in the alloy (1.0 and 1.1 wt.%, Table 1) and are equal to 0.5 and 0.6 wt.%, respectively. The contents of Zn, Ca and Mg in the α-Al solid solution remain almost unchanged after SSHT. Concurrently, the amount of Mg in α-Al solid solution increases from 0.6 to 1.0 wt.%. After SSHT, the Mg content in the α-Al solid solution was equal to its content in the alloy.

The XRD patterns of AlZn3Ca2, AlZn3Ca2Cu1 and AlZn3Ca2Mg1 alloys in as-cast conditions are shown in Fig. 8. All alloys consist of a solid solution of α-Al and an intermediate phase, with diffraction peaks between the Al_4Ca and Al_2CaZn_2 phases. KONO et al [43] reported that Zn can dissolve in significant quantities of Al_4Ca phase, thereby changing its composition to Al_3ZnCa. Later, PANI et al [44] reported a wide homogeneity range of intermediate phase composition from Al_4Ca to $Al_{1.88}CaZn_{2.12}$ at 550 °C. The general formula of this phase was proposed as $Ca(Zn_{1-x}Al_x)_4$ (x=0.47−1.00 at 550 °C) with an Al_4Ba-type structure [44], which is consistent with ternary compound Al_2CaZn_2 [45]. The phase boundaries between Al_4Ca and Al_3CaZn as well as Al_3CaZn and Al_2CaZn_2 are not clearly identified in the literature [43−45]. For convenience, this phase will be referred as $(Al,Zn)_4Ca$ throughout the remaining of the work. Addition of 1 wt.% Cu or 1 wt.% Mg to AlZn3Ca2 alloy did not promote the formation of new phases. However, when 1 wt.% Cu was added to AlZn3Ca2 alloy, the $(Al,Zn)_4Ca$ phase peaks are shifted to higher angles that clearly can be seen on the enlarged part of the XRD pattern. Thus, Cu dissolved in $(Al,Zn)_4Ca$ phase. At the same time the Mg addition does not change the position of $(Al,Zn)_4Ca$ peaks, but little changes the peaks of α-Al, because it dissolves in it mostly. These results are in accordance with the analyses of EDS maps of alloys (Fig. 7).

3.4 Fluidity and hot tearing criterion of Al−Zn−Ca−(Cu,Mg) alloys

Figure 9(a) shows the fluidity of the Al−Zn−Ca−(Cu,Mg) alloys. The lengths of the spiral test probes vary from 182 to 317 mm. The lowest fluidity is typical for the AlZn1Ca2 alloy, which contains the lowest amount of alloying elements and, as a result, low fraction of eutectic in its structure. The increase in the amount of Ca and Zn over 3 wt.% led to a decrease in fluidity. Additions of 1 wt.% Cu and Mg significantly reduced the fluidity of the obtained alloys from 307 to 265 and 252 mm, respectively. The reason for this is the decrease in the fraction of eutectics and the long freezing range. After pouring samples into green sand molds, a gray layer was found on the surface of the spirals, which was formed during the interaction of the melt with water from the mold. According to the XRD pattern, the surface layer consists of CaO and $Al_2(OH)_6{\cdot}H_2O$, as shown in Fig. 10(a). For the alloy with the highest amount of eutectic (AlZn3Ca4), a spiral test was carried out using a furan resin bonded sand mold. The fluidity probe of the AlZn3Ca4 alloy in green sand mold and sand mold with a furan binder is shown in Figs. 10(b, c). It has been found that in the absence of contact between the melt and moisture, the

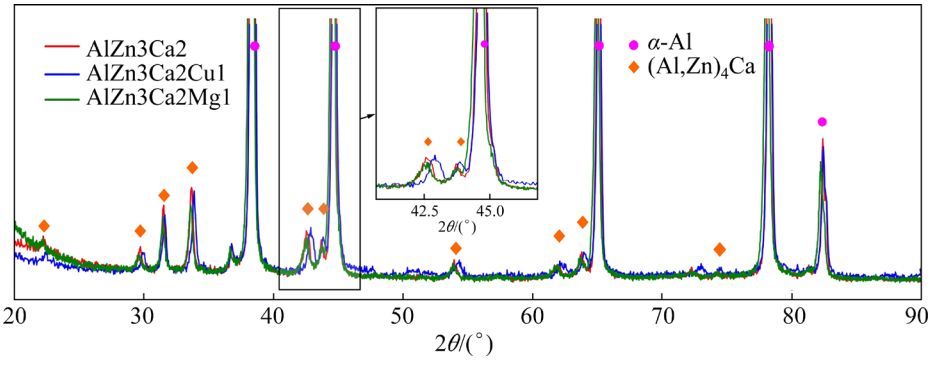

Fig. 8 XRD patterns of AlZn3Ca2, AlZn3Ca2Cu1 and AlZn3Ca2Mg1 alloys in as-cast condition

fluidity of AlZn3Ca4 increased from 260 to 450 mm.

To evaluate the fluidity of the resulting alloys, the results were compared with that of the commercial A356 alloy. The fluidity of A356 when cast into resin (furan) bonded sand mold at a pouring temperature of 740 °C is 710 mm [34]. The resulting fluidity of investigated alloys is lower than that of A356. However, considering the difference in pouring temperature, the fluidity of the alloy does not differ critically. Moreover, for the high pressure die casting method for which the alloys are developed, the less demanding requirements for the alloy fluidity.

The hot tearing criterion of the Al−Zn−Ca−(Cu,Mg) alloys, i.e., the maximum length of the dog-bone branch without tears, is shown in Fig. 9(b). The results of the hot tearing test show that the ternary Al−Zn−Ca alloys without Cu and Mg exhibit the highly hot tearing criterion of ~80 mm and are not susceptible for hot tearing. AlZn3Ca2Cu1 and AlZn3Ca2Mg1 alloys have higher hot tearing susceptibility, especially the latter one. The hot tearing criterion for these alloys are 61 and 25 mm, respectively. The main reason of increasing hot tearing tendency is the long freezing range of these four-component alloys and low fraction of eutectic. In general, most of investigated ternary alloys have a high resistance to hot tearing.

3.5 Thermal conductivity of Al−Zn−Ca−(Cu,Mg) alloys

Figure 11 shows the thermal conductivities (λ) of as-cast and SSHT Al−Zn−Ca−(Cu,Mg) alloys calculated using Eq. (2). The thermal conductivity of the as-cast alloys with different Ca contents of 2, 3, and 4 wt.% are 204, 195, and 183 W/(m·K), respectively. Increasing the Zn content from 1 to 5 wt.% also reduces the thermal conductivity of the alloys from 206 to 196 W/(m·K). The thermal conductivity of the AlZn3Ca2 alloy decreases after alloying with Cu and Mg from 204 to 195 and to 175 W/(m·K), respectively. However, all alloys have a thermal conductivity of at least 75% that of pure Al. After heat treatment, a slight increase in thermal conductivity was observed, particularly in

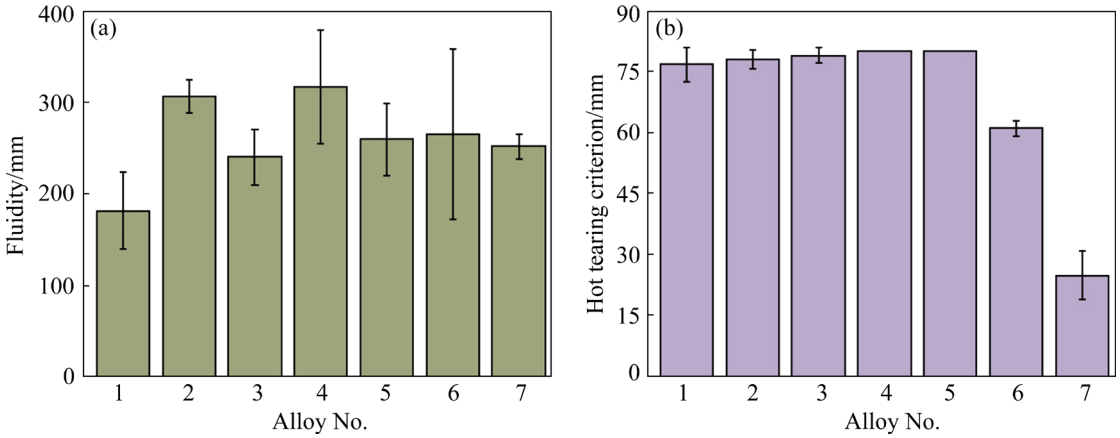

Fig. 9 Fluidity (a) and hot tearing criterion (b) of Al−Zn−Ca alloys

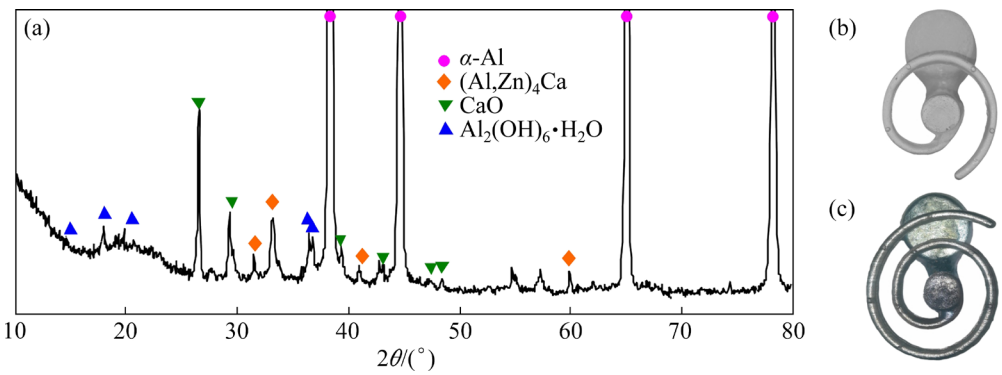

Fig. 10 XRD pattern of surface layer of AlZn3Ca4 alloy (a), and fluidity test spirals cast into green sand mold (b) and sand mold with furan binder (c)

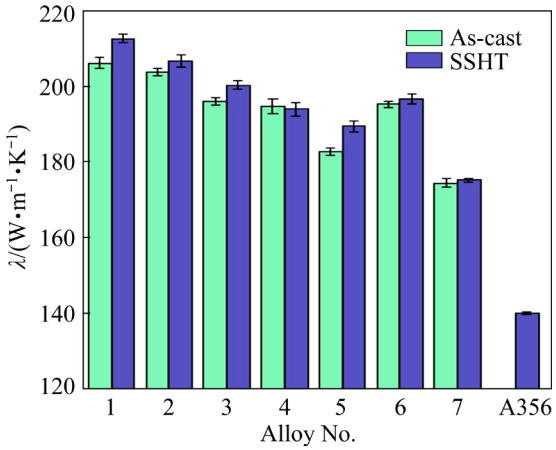

Fig. 11 Thermal conductivity (λ) of Al−Zn−Ca−(Cu,Mg) alloys calculated using Eq. (2)

AlZn1Ca2 and AlZn3Ca4 alloys, which showed an increase of approximately 6 W/(m·K). The increase in thermal conductivity of alloys is likely due to the homogenization of the α-Al solid solution and the change in the morphology of the eutectic phases. Furthermore, heat-treated alloys exhibit a thermal conductivity that is 25%−52% higher than that of the commercial A356 alloy in T4 condition.

The Smith and Palmer equation (Eq. (2)) is an express method for calculating thermal conductivity, but it still has a significant margin of error. Therefore, the thermal conductivity (λ) of the AlZn3Ca3 alloy was also calculated using Eq. (3) based on the results of density (ρ), specific heat capacity (C_p), and thermal diffusivity (a) measurements. The thermal characteristics of the AlZn3Ca3 alloy in the SSHT state are presented in Fig. 12. The data indicate that with increasing temperature, the density and thermal diffusivity decrease while the specific heat capacity increases. The thermal conductivity shows a slight increase from 182.5 W/(m·K) at room temperature to 183.1 W/(m·K) at 139 °C, followed by a rapid decrease to 178.0 W/(m·K) at 300 °C.

3.6 Mechanical properties of Al−Zn−Ca−(Cu,Mg) alloys

The hardness of as-cast alloys increases from HB 33.9 to HB 54.6 as the content of Ca and Zn in the alloys increases, as shown in Fig. 13. Alloying the AlZn3Ca2 alloy with Cu and Mg resulted in an increase in hardness of the as-cast samples from

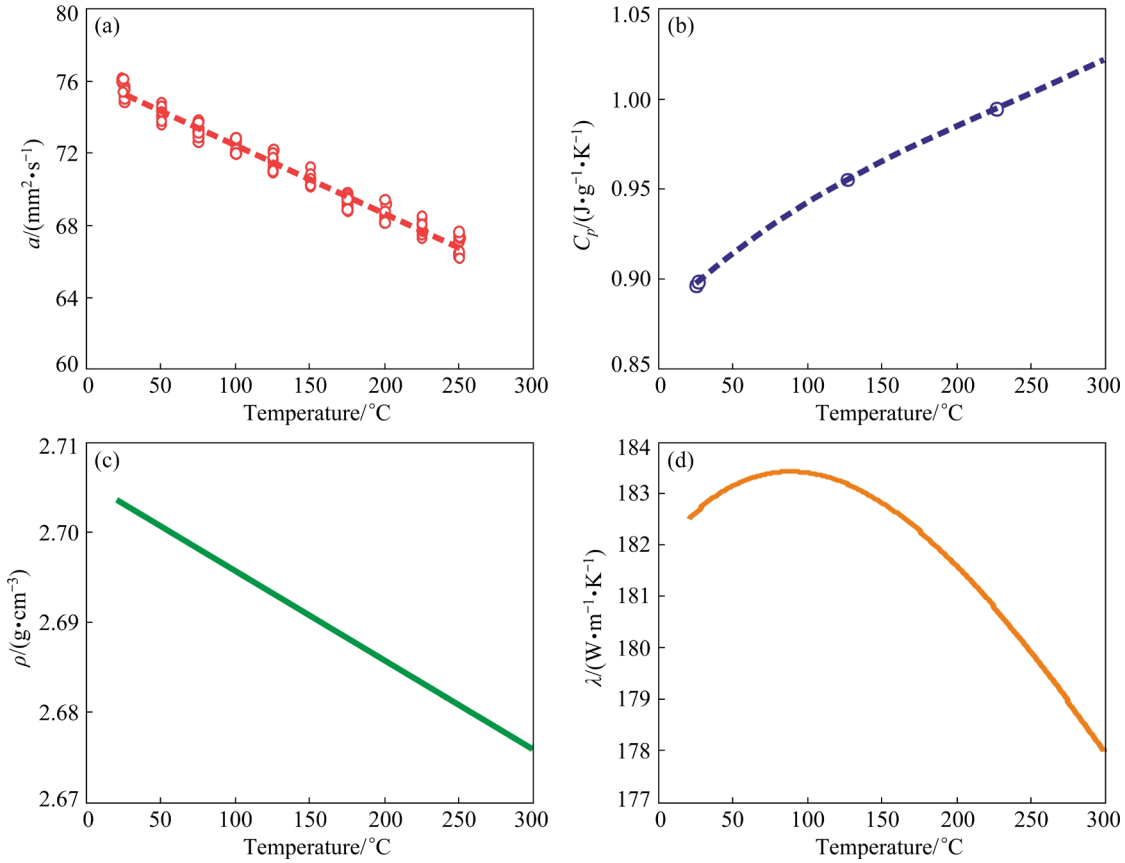

Fig. 12 Thermal properties of AlZn3Ca3 alloy in SSHT state: (a) Thermal diffusivity; (b) Specific heat capacity; (c) Density; (d) Thermal conductivity

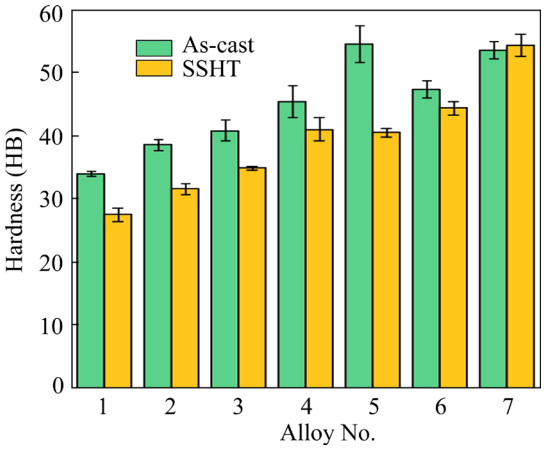

Fig. 13 Hardness of Al−Zn−Ca−(Cu,Mg) alloys

HB 38.5 to HB 47.4 and to HB 53.2, respectively. This is likely due to the dissolution of Cu and Mg in the α-Al solid solution. The heat treatment resulted in a reduction in the hardness of the majority of alloys by HB 3−14. The exception was the AlZn3Ca2Mg1 alloy whose hardness remained the same.

Figure 14 shows the engineering stress−strain curves, ultimate tensile strength (UTS), yield strength (YS), and elongation at fracture (El) of SSHT alloys. The UTS increases from 94 to 114 MPa with an increase of Zn from 1 to 5 wt.%. Similarly, an increase of Ca from 2 to 4 wt.% results in an increase in UTS from 101 to 126 MPa. Additionally, alloying with 1 wt.% of Cu and Mg promotes an increase in UTS from 101 to 135 and 160 MPa, respectively. The YS varies similarly to the tensile strength, depending on the type and content of alloying elements, ranging from 40 to 60 MPa. According to Fig. 14(c), the presented group of alloys has a high El of 13%−27%. Since heat treatment did not increase the hardness of the alloys, it can be assumed that strengths of alloys in the as-cast state are approximately the same as those after SSHT.

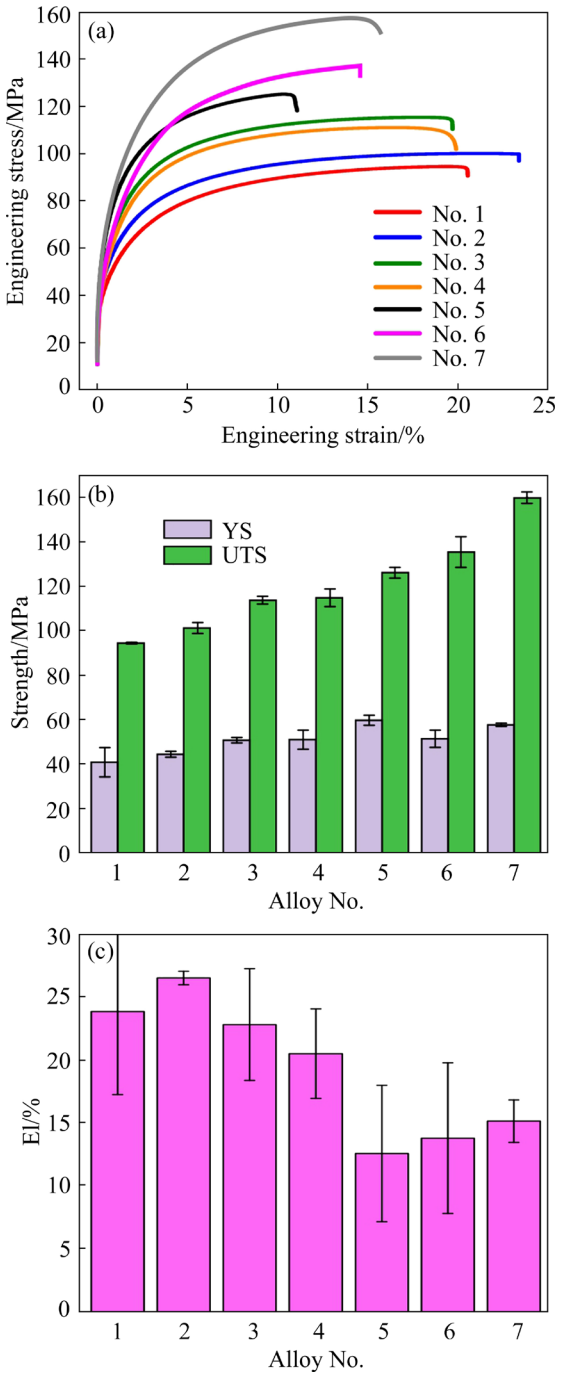

Fig. 14 Mechanical properties of Al−Zn−Ca−(Cu,Mg) alloys in SSHT condition

3.7 Corrosion resistance of Al−Zn−Ca−(Cu,Mg) alloys

Corrosion rates of the Al−Zn−Ca−(Cu,Mg) alloys in the as-cast and SSHT conditions via immersion corrosion test in 5.7% NaCl + 0.3% H_2O_2 with distilled water solution are shown in Fig. 15. Due to the small corrosion rates (CR) and a small number of samples, the error bars are large especially for as-cast samples. It can be concluded that all alloys except AlZn3Ca2Cu1 have a very high corrosion resistance. The CR of most as-cast alloys is 0.006−0.021 mm/a, and the CR of heat-treated alloys is 0.004−0.015 mm/a. Increasing Zn in the as-cast alloys leads to a slight decrease in the CR, while at the same time, an increase in Ca leaves the CR practically unchanged. The CR for an alloy with the addition of Cu in the as-cast and heat-treated state is 1.84 and 1.21 mm/a,

respectively. For all alloys except AlZn3Ca2Cu1, heat treatment contributed to a decrease in the intensity of corrosion process. The CR of A356 alloy in a similar medium is 1.88 mm/a. Thus, although the corrosion rate of AlZn3Ca2Cu1 is higher than that of other alloys, it is still approximately equal to A356 alloy.

Figure 16 shows the panoramic cross-sectional images of AlZn3Ca2, AlZn3Ca2Cu1 and A356 alloys in SSHT condition after immersion corrosion tests. The surface of AlZn3Ca2Cu1 showed that the highest CR, after the corrosion test was covered with deep corrosion cavities up to ~360 μm (as-cast) and up to ~270 μm (SSHT state) in size. At the same time, the result obtained is not inferior to the industrial alloy A356 (SSHT state), whose corrosion cavities are ~320 μm. The depth of corrosion cavities of other alloys did not exceed ~130 μm in as-cast condition and ~170 μm after SSHT. At the same time, if AlZn3Ca2Cu1 and A356 alloys are characterized by multiple corrosion cavities of the entire surface, then in other alloys, corrosion cavities are rare and are found in small quantities. Moreover, for most of the studied alloys and A356, micro galvanic corrosion proceeds along the eutectic phase, which in this case is acting as anode with respect of α-Al. According to Figs. 16(d−f), for the AlZn3Ca2Cu1 alloy, the eutectic phase became the cathode with respect to α-Al due to the copper presence in the eutectic phase; therefore, corrosion was localized in the Al solid solution [46].

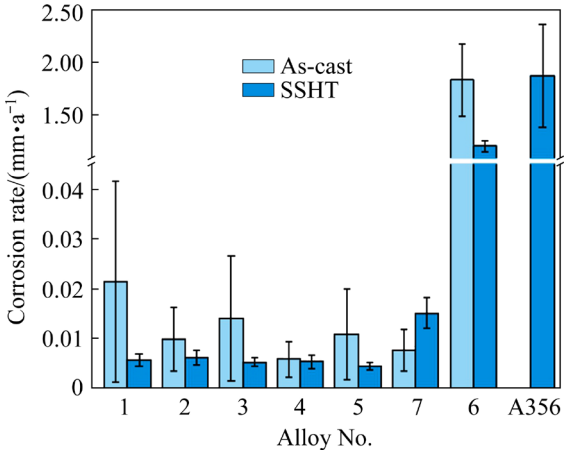

Fig. 15 Corrosion rate of Al−Zn−Ca−(Cu,Mg) alloys by immersion corrosion test

Typical polarization curves obtained in 5.7% NaCl + 0.3% H_2O_2 aqueous solution for the Al−Zn−Ca−(Cu,Mg) alloys in as-cast state and after T4 SSHT are shown in Fig. 17. The corrosion characteristics of alloys, including corrosion current density (J_{corr}), corrosion potential (φ_{corr}) and corrosion rate (CR) were calculated using Tafel fitting. The results of electrochemical corrosion tests are presented in Table 4. The anodic branch of the polarization curve exhibits typical resistive behavior due to the formation of a layer of corrosion products, while the cathodic branch of the polarization curve exhibits typical and expected diffusion control behavior for all alloys except AlZn3Ca2Cu1. It can be seen that φ_{corr} of ternary alloys in the as-cast state varies from −1.0 to −1.1 V. The addition of Mg has practically no effect on the corrosion potential, while Cu leads to the positive shift φ_{corr} by more than 0.3 V. In the as-cast state, J_{corr} and CR decrease with increasing Zn, and conversely, an increase in Ca contributes to an increase in J_{corr}. Mg has practically no effect on J_{corr}, while Cu increases it by more than an order of magnitude. After heat treatment, φ_{corr} of most alloys remained almost unchanged. However, for some ternary alloys it began to reach −1.2 V (AlZn1Ca2 and AlZn3Ca4). After SSHT, J_{corr} and CR increased as the Zn and Ca content increased. Simultaneously, J_{corr} of numerous alloys shows a significant increase

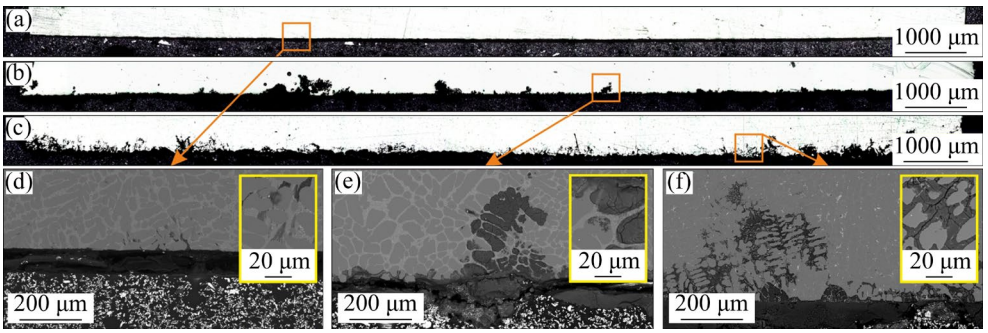

Fig. 16 Panoramic cross-sectional images (a–c) and cross-sectional microstructures (d–f) of SSHT samples: (a, d) AlZn3Ca2; (b, e) AlZn3Ca2Cu1; (c, f) A356 alloy after immersion corrosion

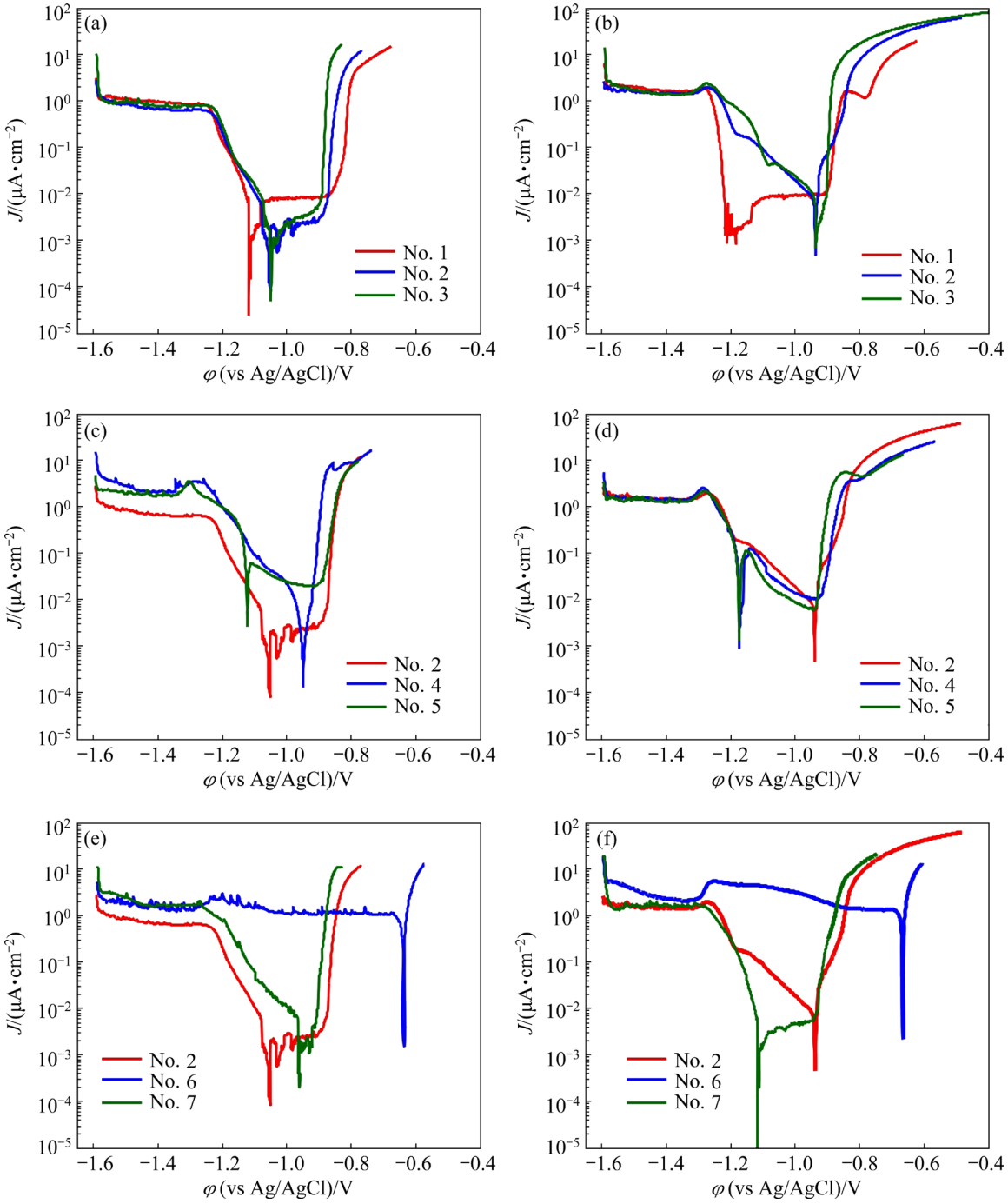

Fig. 17 Polarization curves of as-cast (a, c, e) and SSHT (b, d, f) Al−Zn−Ca−(Cu,Mg) alloys in 5.7% NaCl + 0.3% H_2O_2 aqueous solution

in comparison to that for as-cast alloys. As a result, CR of SSHT alloys is greater than that of as-cast alloys.

4 Discussion

Multicomponent aluminum alloys may contain alloying elements in two states: solutions and/or precipitated compounds. It is believed that elements dissolved in the α-Al matrix have a more negative effect on the alloys conductivity than those out of solution [13,47−49]. The study shows that the thermal conductivity of binary alloys is less affected by the addition of elements that are practically insoluble in Al solid solution, such as Ca, Y, Gd, La, Ni, and Fe, compared to the effect of

Table 4 Electrochemical corrosion test data obtained for as-cast and T4 heat-treated Al−Zn−Ca−(Cu,Mg) alloys in 5.7% NaCl + 0.3% H_2O_2 aqueous solution corrosion media

Alloy No.	φ (vs Ag/AgCl)/V		J_{cor}/(μA·cm^{-2})		Corrosion rate/(mm·a^{-1})	
	As-cast	SSHT	As-cast	SSHT	As-cast	SSHT
1	–1.11	–1.17	4.35	3.42	0.049	0.038
2	–0.99	–0.98	1.71	6.65	0.019	0.075
3	–1.06	–1.05	0.96	7.27	0.011	0.082
4	–0.96	–1.13	1.47	6.52	0.017	0.074
5	–1.12	–1.16	11.22	8.09	0.130	0.093
6	–0.65	–0.67	56.45	191.12	0.635	2.149
7	–0.94	–1.05	1.30	2.01	0.015	0.023

adding Mg, Ti, Mn, Cu, Zn, Si, Zr, and Cr. Thus, the purity of α-Al is a crucial factor in the heat transfer efficiency of an aluminum alloy. Additionally, RE had minimal impact on the thermal conductivity of aluminum because these elements are typically found in the form of compounds, which helps maintain the high purity of α-Al and does not impede the movement of electrons and phonons [8,13,48,50]. It is important to note that although there is a small region of calcium solubility in α-Al, the atomic radius of this element differs from that of aluminum by approximately 40%, while the atomic radii of the other elements studied do not differ as much (about 10%) [51]. Thus, the Al−Ca binary alloy exhibited superior conductivity compared to Al−Fe or Al−Ni.

The Al−Zn−Ca−(Cu,Mg) alloys in their as-cast state consist of α-Al dendrites and a lamellar eutectic of α-Al+$(Al,Zn)_4Ca$. Zn, Mg and Cu are presented both in α-Al and $(Al,Zn)_4Ca$ phases, but in $(Al,Zn)_4Ca$ the content of Zn, Mg and Cu is high. Cu and Mg decrease thermal conductivity of α-Al with great extent due to the higher lattice mismatch parameters for Al−Cu(−13.2%) and Al−Mg(10.8%) solid solutions compared to Al−Zn(−3.2%) [52]. However, increasing the Ca content of alloys leads to a decrease in conductivity, despite the fact that this element is almost insoluble in aluminum solid solution. This reduction in thermal conductivity corresponds to a change in the fraction of eutectic in the alloys, as shown in Fig. 6(a). This correlation can be attributed to the increase in second phase content and the creation of additional phase boundaries, which leads to lattice distortion and hinder the free movement of electrons and phonons [11,53].

After SSHT, the lamellas of $(Al,Zn)_4Ca$ acquire a more compact shape and increase in size. The coarsening and spheroidization of the $(Al,Zn)_4Ca$ phase are associated with a decrease in the total α-Al/$(Al,Zn)_4Ca$ interfacial area [54]. During the SSHT, Ca or Zn atoms begin to diffuse from positions with large curvatures (tips) to flat interfaces. This process causes the tips to dissolve, resulting in the gradual blunting of the edges of the $(Al,Zn)_4Ca$ particles. Apparently, these structural changes resulted in an increase in thermal conductivity of alloys. Previous studies [55–57] have demonstrated that altering the shape of eutectic silicon from lamellar and/or acicular to fibrous can enhance the thermal conductivity of Al−Si alloys. CHEN et al [9] found that alloys with closely distributed fine plate-shaped silicon precipitates have lower thermal conductivity than those with larger distances between precipitates. Thus, the increase in thermal conductivity of Al−Zn−Ca alloys was achieved by spheroidization and growth of $(Al,Zn)_4Ca$ particles providing sufficient distance between the precipitates, allowing for free movement of electrons. However, during heat treatment, increasing the Mg content of α-Al by approximately two times is observed (see Fig. 6(b)). Thus, the thermal conductivity of containing-Mg alloy remained unchanged after SSHT.

The thermal conductivity of the AlZn3Ca3 alloy firstly slightly increased and then decreased as the temperature increased. This phenomenon for aluminum alloys has been previously noted in studies [58,59]. It is noteworthy that the slight increase in thermal conductivity of the AlZn3Ca3 alloy in the range from room temperature to approximately 140 °C corresponds to the dependence observed for pure Al [59]. The thermal conductivity of the AlZn3Ca3 alloy was calculated using the Smith and Palmer equation to be approximately 194.0 W/(m·K), which is 6% higher than that obtained using LFA and DIL data (~182.6 W/(m·K)). This minor difference confirms the reliability of the results.

The increasing of Ca and Zn up to 3 wt.% leads to an increase of the fluidity of alloys. This phenomenon is directly related to the increase of

the eutectic amount in the alloys structure. It is a well-known fact that the fluidity of ternary alloys increases as the freezing range decreases and approaches the eutectic point of the phase diagram [60]. However, in alloys with Zn and Ca content higher than 3 wt.%, the fluidity is decreased. According to calculations in the Thermo-Calc program, the decrease of fluidity in the AlZn5Ca2 alloy may be due to a slight increase in the freezing range from 49 to 55 °C in comparison with the AlZn3Ca2 alloy. When Ca is in large quantities in alloy, and mold contains large amount of moisture, the Ca-rich oxide film composed of CaO and $Al_2(OH)_6{\cdot}H_2O$ is observed. However, when the spiral probes were poured into furan resin sand molds with low moisture, the resulting castings had a metallic sheen and this type of mold provided high fluidity. This is because the Ca-rich oxide film hindered the movement of the melt in the mold cavity. Dense oxide films are known to impede the filling of mold spaces, particularly narrow channels, and reduce the fluidity of alloys [60,61]. Additionally, green sand molds have a higher cooling capacity than furan resin sand molds [62]. The addition of copper and magnesium increase the freezing range and decrease the fraction of eutectic. These changes have a negative impact on the fluidity and hot tearing resistance of the investigated alloys.

The main mechanisms of strengthening of casting aluminum alloys are dispersion strengthening and solid solution strengthening [63−66]. The solid solution strengthening is contributed by the Zn, Cu, and Mg contents in the studied alloys. The main effect of strengthening is achieved due to the difference in atomic size and/or shear modulus between the alloying elements and the Al matrix [67]. Increasing the amount of Zn, Cu, and Mg in α-Al leads to increase of hardness in the alloys. It is worth noting that the increase in hardness with the addition of Mg and Cu is greater than that with the addition of Zn. This is probably due to the greater deviation of the atomic radii of Cu (1.28 Å) and Mg (1.60 Å) from Al (1.43 Å) than that of Zn(1.34 Å) [68]. Additionally, an increase in hardness was observed with increasing Ca, likely due to an increase in the amount of the $(Al,Zn)_4Ca$ phase. After SSHT, hardness of most alloys was decreased. This is attributed the the microstructural changes described earlier.

The low mechanical properties of Al−Zn−Ca−(Cu,Mg) alloys are observed. It is known that the smaller the particles and the denser their arrangement in the structure, the higher the strength of the alloy [61,69]. Therefore, the low strength exhibited by Al−Zn−Ca−(Cu,Mg) alloys is attributed to the morphology of $(Al,Zn)_4Ca$ particles and the weak strengthening of the solid solution. At the same time, the spheroidization of $(Al,Zn)_4Ca$ particles provided high ductility of the alloys, resulting in an EI of more than 13% [24,25]. Future research will aim to enhance the mechanical properties of Al−Zn−Ca system alloys while maintaining high thermal conductivity and corrosion resistance. To achieve this, small amounts of Sc and Zr will be used.

Most of the studied alloys exhibited high corrosion resistance in both the as-cast and heat-treated states. The $(Al,Zn)_4Ca$ phase, formed by eutectic reaction and located on the dendritic cell boundaries, preferentially dissolves during corrosion process because it acts as a anode with respect to α-Al, due to the higher electronegativity of Zn and Ca compared to Al. The lamellar structure formed by the $(Al,Zn)_4Ca$ phase along the grain boundaries improves the corrosion resistance. When corrosion process starts the corrosion products are firmly held in the interdendritic space and no spallation of corrosion products is observed which inhibits corrosion. The AlZn3Ca2Cu1 alloy was the only exception, with corrosion rate approximately 100 times higher than for other alloys, as shown by the results of the immersion corrosion test. Since Cu dissolves to a greater extent in the eutectic $(Al,Zn)_4Ca$ particles, the eutectic acts as a preferential cathode with respect to α-Al, causing that galvanic pairs are formed at the phase boundary between Cu-rich areas and the Al matrix in an aqueous electrolyte solution containing an activator ion (Cl^-), leading to the development of local foci of corrosion [70−72]. When the results of immersion tests were compared, the corrosion resistance of Al−Zn−Ca−(Mg) alloys was hundreds of times higher than that of the widely used commercial alloy A356. Thus, it can be concluded that Al−Zn−Ca−(Mg) alloys are characterized by very high corrosion resistance in NaCl solution.

The obtained corrosion rate for most of investigated alloys in the electrochemical test is higher than that in the immersion test. The

corrosion rate of the AlZn3Ca4 alloy varies especially greatly (0.01 mm/a for immersion, 0.13 mm/a for electrochemical corrosion measurements). The lower corrosion rate during immersion testing may be due to a decrease in the intensity of the corrosion process and limited corrosion development caused by the protective barrier effect of corrosion products.

5 Conclusions

(1) The influence of alloying elements on the thermal conductivity of Al was analysed. The alloying elements are arranged in order of their degree of reduction in thermal conductivity as follows: Gd, La, Y, Zn, Ca, Mg, Cu, Ni, Fe, Si, Ti, Zr, Mn, and Cr. The primary factors that decrease the thermal conductivity of aluminum are the solubility of alloying elements in the α-Al solid solution and the degree of difference in the atomic radii of the elements and Al. The Al−Zn−Ca−(Cu,Mg) system was selected because Zn, Cu, and Mg reduce the thermal conductivity of the α-Al solid solution to a lesser extent, and Ca being practically insoluble in Al.

(2) The structure of all Al−Zn−Ca−(Cu,Mg) alloys consists of α-Al and eutectic, which contains a $(Al,Zn)_4Ca$ phase. The equilibrium freezing range for Al−(1−5)wt.%Zn−(2−4)wt.%Ca−(1wt.%Cu,Mg) alloys is ~50 °C, doubling under non-equilibrium conditions. Cu or Mg increases the non-equilibrium freezing range up to 170 °C. Heat treatment (500 °C, 5 h and 550 °C, 5 h + quenching in water) leads to fragmentation of eutectic lamellas of the $(Al,Zn)_4Ca$ phase, their spheroidization and growth up to ~3 μm.

(3) Compared to A356 aluminum alloy, the Al−Zn−Ca−(Cu,Mg) alloys showed low fluidity (182−317 mm), but their resistance to hot tearing was high. Mg negatively affects hot tearing resistance of alloys. Upon contact with moisture contained in the green sand mold, a light gray oxide layer consisting of CaO and $Al_2(OH)_6{\cdot}H_2O$ is formed on the surface of the casting that reduces the fluidity of the alloys.

(4) The thermal conductivity of as-cast Al−Zn−Ca−(Cu,Mg) alloys is 175−206 W/(m·K), which is at least 75% of pure Al conductivity. This is attributed to the low content of dissolved elements in the α-Al solid solution. Hardness in as-cast state is HB 33.9−54.6. Heat treatment slightly increases conductivity and reduces hardness by HB 3−14.

(5) Tensile tests show that strength increases with increasing Zn and Ca. UTS and YS are (94−160) MPa and (40−60) MPa, respectively. However, alloys have high elongation at fracture of >15%.

(6) Corrosion rate in 5.7% NaCl + 0.3% H_2O_2 obtained by the immersion corrosion test is less than 0.02 mm/a for most of alloys, which is about 1% that of A356 (~1.9 mm/a). AlZn3Ca2Cu1 has the worst corrosion resistance (1.2 mm/a). Electrochemical corrosion tests results confirm high corrosion resistance of alloys, slightly reduced by heat treatment.

CRediT authorship contribution statement

A. A. LYSKOVICH: Methodology, Investigation, Formal analysis, Writing – Original draft, Writing – Review & editing; **V. E. BAZHENOV:** Conceptualization, Project administration, Data curation, Writing – Review & editing, Funding acquisition; **I. I. BARANOV:** Investigation; **V. A. BAUTIN:** Investigation, Writing − Review & editing, Validation; **A. V. SANNIKOV:** Investigation; **A. I. BAZLOV:** Investigation, Writing − Review & editing, Validation; **E. I. TIAN:** Investigation; **A. A. STEPASHKIN:** Investigation; **A. V. KOLTYGIN:** Methodology, Project administration, Validation; **V. D. BELOV:** Resources, Supervision.

Declaration of competing interest

The authors declare that they have no known competing financial interests or personal relationships that could have appeared to influence the work reported in this paper.

Acknowledgments

This research was supported by the Russian Science Foundation (No. 24-29-00682, https://rscf.ru/project/24-29-00682/).

References

[1] SOUISSI N, SOUISSI S, LE NINIVEN C, AMAR M B, BRADAI C, ELHALOUANI F. Optimization of squeeze casting parameters for 2017 A wrought Al alloy using Taguchi method [J]. Metals, 2014, 4: 141−154. https://doi.org/10. 3390/met4020141.

[2] MILLER W S, ZHUANG L, BOTTEMA J, WITTEBROOD A J, de SMET P, HASZLER A, VIEREGGE A. Recent development in aluminium alloys for the automotive industry [J]. Materials Science and Engineering: A, 2000, 280: 37−49. https://doi.org/10.1016/S0921-5093(99)00653-X.

[3] DAVIS J R. Aluminum and aluminum alloys [M]. Materials Park, USA: ASM International, 1993.

[4] JOU R. Y. Thermal analysis of LED heat sinks by high-vacuum die casting (HVDC) [J]. Advanced Science Letters, 2012, 8, 1: 421−426. https://doi.org/10.1166/asl.2012.2393.

[5] BASER T A, UMAY E, AKINCI V. New trends in aluminum die casting alloys for automotive applications [J]. The Eurasia Proceedings of Science Technology Engineering and Mathematics, 2022, 21: 79−87. https://doi.org/10.55549/epstem.1227541.

[6] SCE A, CAPORALE L. High density die casting (HDDC): new frontiers in the manufacturing of heat sinks [J]. Journal of Physics: Conference Series. – IOP Publishing, 2014, 525: 1: 012020. https://doi.org/10.1088/1742-6596/525/1/012020.

[7] KARABAY S. Modification of AA-6201 alloy for manufacturing of high conductivity and extra high conductivity wires with property of high tensile stress after artificial aging heat treatment for all-aluminium alloy conductors [J]. Materials & Design, 2006, 27: 821−832. https://doi.org/10.1016/j.matdes.2005.06.005.

[8] ZIMAN J M. Electrons and phonons: The theory of transport phenomena in solids [M]. Oxford: Oxford University Press, 2001.

[9] CHEN J K, HUNG H Y, WANG C F, TANG N K. Effects of casting and heat treatment processes on the thermal conductivity of an Al−Si−Cu−Fe−Zn alloy [J]. International Journal of Heat and Mass Transfer, 2017, 105: 189−195. https://doi.org/10.1016/j.ijheatmasstransfer.2016.09.090.

[10] VANDERSLUIS E, LOMBARDI A, RAVINDRAN C, BOIS-BROCHU A, CHIESA F, MACKAY R. Factors influencing thermal conductivity and mechanical properties in 319 Al alloy cylinder heads [J]. Materials Science and Engineering: A, 2015, 648: 401−411. https://doi.org/10.1016/j.msea.2015.09.091.

[11] KUMAR L, JANG J C, YU H, SHIN K S. Effect of secondary phase on mechanical and thermal conductivity of Al−Si−*x*Fe−Mg−*y*Cu−Mn die casting alloys [J]. Materials Letters, 2022, 314: 131889. https://doi.org/10.1016/j.matlet.2022.131889.

[12] IKHMAYIES S. Phase diagrams of Al−Si system [C]// Energy Technology 2019: Carbon Dioxide Management and Other Technologies. Cham: Springer International Publishing, 2019: 231−237.

[13] ZHANG A L, LI Y X. Effect of alloying elements on thermal conductivity of aluminum [J]. Journal of Materials Research, 2023, 38: 2049−2058. https://doi.org/10.1557/s43578-023-00942-w.

[14] CHEN J K, HUNG H Y, WANG C F, TANG N K. Thermal and electrical conductivity in Al−Si/Cu/Fe/Mg binary and ternary Al alloys [J]. Journal of Materials Science, 2015, 50: 5630−5639. https://doi.org/10.1007/s10853-015-9115-9.

[15] ZHANG A L, LI Y X. Thermal conductivity of aluminum alloys—A review [J]. Materials, 2023, 16: 2972. https://doi.org/10. 3390/ma16082972.

[16] PAN H C, PAN F S, YANG R M, PENG J, ZHAO C Y, SHE J, GAO Z Y, TANG A T. Thermal and electrical conductivity of binary magnesium alloys [J]. Journal of Materials Science, 2014, 49: 3107−3124. https://doi.org/10.1007/s10853-013-8012-3.

[17] BAZHENOV V E, KOLTYGIN A V, SUNG M C, PARK S H, TITOV A Y, BAUTIN V A, MATVEEV S V, BELOV M V, BELOV V D, MALYUTIN K V. Design of MgZnSiCa casting magnesium alloy with high thermal conductivity [J]. Journal of Magnesium and Alloys, 2020, 8: 184−191. https://doi.org/10.1016/j.jma.2019.11.008.

[18] BAZHENOV V E, KOLTYGIN A V, SUNG M C, PARK S H, TSELOVALNIK Y V, STEPASHKIN A A, RIZHSKY A A, BELOV M V, BELOV V D, MALYUTIN K V. Development of Mg−Zn−Y−Zr casting magnesium alloy with high thermal conductivity [J]. Journal of Magnesium and Alloys, 2021, 9: 1567−1577. https://doi.org/10.1016/j.jma.2020.11.020.

[19] BELOV N A, NAUMOVA E A, ALABIN A N, MATVEEVA I A. Effect of scandium on structure and hardening of Al−Ca eutectic alloys [J]. Journal of Alloys and Compounds, 2015, 646: 741−747. https://doi.org/10.1016/j.jallcom.2015.05.155.

[20] AKOPYAN T K, LETYAGIN N V, SVIRIDOVA T Y A, KOROTKOVA N O, PROSVIRYAKOV A S. New casting alloys based on the Al+Al_4(Ca,La) eutectic [J]. JOM, 2020, 72: 3779−3786. https://doi.org/10.1007/s11837-020-04340-z.

[21] HOU S L, LIU P P, ZHANG D, ZHANG J S, ZHUANG L Z. Precipitation hardening behavior and microstructure evolution of Al−5.1Mg−0.15Cu alloy with 3.0Zn (wt%) addition [J]. Journal of Materials Science, 2018, 53: 3846−3861. https://doi.org/10.1007/s10853-017-1811-1.

[22] GUO C, ZHANG H T, LI S S, CHEN R X, NAN Y E, LI L, WANG P, LI B M, CUI J Z, NAGAUMI H. Evolution of microstructure, mechanical properties and corrosion behavior of Al−4Mg−2Zn–0.3Ag (wt.%) alloy processed by T6 or thermomechanical treatment [J]. Corrosion Science, 2021, 188: 109551. https://doi.org/10.1016/j.corsci.2021.109551.

[23] BEROUAL S, BOUMERZOUG Z, PAILLARD P, BORJON-PIRON Y. Effects of heat treatment and addition of small amounts of Cu and Mg on the microstructure and mechanical properties of Al−Si−Cu and Al−Si−Mg cast alloys [J]. Journal of Alloys and Compounds, 2019, 784: 1026−1035. https://doi.org/10.1016/j.jallcom.2018.12.365.

[24] SHVETS' V A, LAVRENKO V O, TALASH V M. Experience of application of protectors made of Al−Zn−Ca alloys [J]. Materials Science, 2006, 42: 563−565. https://doi.org/10.1007/s11003-006-0115-4.

[25] DANG Z L, ZHAN Y Z, PANG M J, WANG H Z, DU Y. Structural, electronic, elastic and thermodynamic properties of CaAl2Zn2 compound under different pressures [J]. Computational Materials Science, 2012, 59: 33−40. https://doi.org/10.1016/j.commatsci.2012.02.017.

[26] NAUMOVA E A. Use of calcium in alloys: From modifying to alloying [J]. Russian Journal of Non-Ferrous Metals, 2018, 59: 284−298. https://doi.org/10.3103/S1067821218030100.

[27] BELOV N A, NAUMOVA E A, AKOPYAN T K. Effect of calcium on structure, phase composition and hardening of Al−Zn−Mg alloys containing up to 12wt.%Zn [J]. Materials Research, 2015, 18: 1384−1391. https://doi.org/10.1590/1516-1439.036415.

[28] NAUMOVA E A, BELOV N A, BAZLOVA T A. Effect of heat treatment on structure and strengthening of cast eutectic aluminum alloy Al9Zn4Ca3Mg [J]. Metal Science and Heat Treatment, 2015, 57: 274−280. https://doi.org/10.1007/s11041-015-9874-6.

[29] ANDERSSON J O, HELANDER T, HÖGLUND L, SHI P F, SUNDMAN B. Thermo-Calc & DICTRA, computational tools for materials science [J]. Calphad, 2002, 26: 273−312. https://doi.org/10.1016/S0364-5916(02)00037-8.

[30] Thermo-Calc Software TCAL4: TCS Al-based alloy database [EB/OL]. 2015. http://www.thermocalc.com.

[31] ZHENG X, CAHILL D G, KRASNOCHTCHEKOV P, AVERBACK R S, ZHAO J C. High-throughput thermal conductivity measurements of nickel solid solutions and the applicability of the Wiedemann−Franz law [J]. Acta Materialia, 2007, 55: 5177−5185. https://doi.org/10.1016/j.actamat.2007.05.037.

[32] KLEMENS P G, WILLIAMS R K. Thermal conductivity of metals and alloys [J]. International Metals Reviews, 1986, 31: 197−215. https://doi.org/10.1179/imtr.1986.31.1.197.

[33] Properties and selection: Nonferrous alloys and special-purpose materials [M]. Materials Park, USA: ASM International, 2002.

[34] BAZHENOV V E, PETROVA A V, KOLTYGIN A V. Simulation of fluidity and misrun prediction for the casting of 356.0 aluminum alloy into sand molds [J]. International Journal of Metalcasting, 2018, 12: 514−522. https://doi.org/10.1007/s40962-017-0188-x.

[35] CHASE M W. NIST-JANAF thermochemical tables [J]. Journal of Physical and Chemical Reference Data, 1998, 9: 1-1951.

[36] ASTM standard G110−92. Standard practice for evaluating intergranular corrosion resistance of heat treatable aluminum alloys by immersion in sodium chloride + hydrogen peroxide solution [S]. West Conshohocken: ASTM International, 2003.

[37] ASTM standard G1−03. Standard practice for preparing, cleaning, and evaluating corrosion test specimens [S]. West Conshohocken: ASTM International, 2011. https://doi.org/10.1asn520/G0001-03R17E01.

[38] ASTM standard G102−89. Standard practice for calculation of corrosion rates and related information from electrochemical measurements [S]. West Conshohocken: ASTM International, 2015. https://doi.org/10.1520/G0102-89R15E011.

[39] POZDNYAKOV A V, BARKOV R Y. Effect of impurities on the phase composition and properties of a new alloy of the Al−Y−Er−Zr−Sc system [J]. Metallurgist, 2019, 63: 79−86. https://doi.org/10.1007/s11015-019-00796-w.

[40] POZDNIAKOV A V, BARKOV R Y, AMER S M, LEVCHENKO V S, KOTOV A D, MIKHAYLOVSKAYA A V. Microstructure, mechanical properties and superplasticity of the Al−Cu−Y−Zr alloy [J]. Materials Science and Engineering: A, 2019, 758: 28−35. https://doi.org/10.1016/j.msea.2019.04.118.

[41] PEKGULERYUZ M O, LIN S, OZBAKIR E, TEMUR D, ALIRAVCI C. Hot tear susceptibility of aluminium–silicon binary alloys [J]. International Journal of Cast Metals Research, 2010, 23: 310−320. https://doi.org/10.1179/136404610X12738456167267.

[42] ULUDAĞ M, ÇETIN R, DISPINAR D. Freezing range, melt quality, and hot tearing in Al−Si alloys [J]. Metallurgical and Materials Transactions A, 2018, 49: 1948−1961. https://doi.org/10.1007/s11661-018-4512-8.

[43] KONO N, TSUCHIDA Y, MUROMACHI S, WATANABE H. Study of the Al−Ca−Zn ternary phase diagram [J]. Journal of Japan Institute of Light Metals, 1985, 35: 574−580.

[44] PANI M, FORNASINI M L, MAZZONE D, MERLO F. Structural features of intermetallic phases in the Ca−Zn−Al system [J]. Zeitschrift Für Kristallographie, 2009, 224: 397−406. https://doi.org/10.1524/zkri.2009.1173.

[45] KONICA S. Experimental investigation of the A−Ca−Zn system [D]. Quebec, Canada: Concordia University Montreal, 2013.

[46] BETHENCOURT M., BOTANA F J, CANO M J, MARCOS M, SÁNCHEZ-AMAYA J M, GONZÁLEZ-ROVIRA L. Behaviour of the alloy AA2017 in aqueous solutions of NaCl. Part I: Corrosion mechanisms [J]. Corrosion Science, 2009, 51: 518−524. https://doi.org/10.1016/j.corsci.2008.12.027.

[47] VANDERSLUIS E, RAVINDRAN C. Influence of solidification rate on the microstructure, mechanical properties, and thermal conductivity of cast A319 Al alloy [J]. Journal of Materials Science, 2019, 54: 4325−4339. https:// doi.org/10.1007/s10853-018-3109-3.

[48] MUJAHID M, ENGEL N N, CHIA E H. Effect of alloying elements on the conductivity of aluminum alloys [J]. Scripta Metallurgica, 1979, 13: 887−893. https://doi.org/10.1016/0036-9748(79)90181-9.

[49] KIM C W, CHO J I, CHOI S W, KIM Y C. The effect of alloying elements on thermal conductivity of aluminum alloys in high pressure die casting [J]. Advanced Materials Research, 2013, 813: 175−178. https://doi.org/10.4028/www.scientific.net/AMR.813.175.

[50] CHO Y H, KIM H W, LEE J M, KIM M S. A new approach to the design of a low Si-added Al−Si casting alloy for optimising thermal conductivity and fluidity [J]. Journal of Materials Science, 2015, 50: 7271−7281. https://doi.org/10.1007/s10853-015-9282-8.

[51] SLATER J C. Atomic radii in crystals [J]. The Journal of Chemical Physics, 1964, 41: 3199−3204. https://doi.org/10.1063/1.1725697.

[52] UESUGI T, HIGASHI K. First-principles studies on lattice constants and local lattice distortions in solid solution

aluminum alloys [J]. Computational Materials Science, 2013, 67: 1−10. https://doi.org/10.1016/j.commatsci.2012.08.037.

[53] WANG Y, KANG H J, GUO Y, CHEN H T, HU M L, JI Z S. Design and preparation of aluminum alloy with high thermal conductivity based on CALPHAD and first-principles calculation [J]. China Foundry, 2022, 19: 225−237. https://doi.org/10.1007/s41230-022-1122-2.

[54] YU H C, WANG H Y, CHEN L, ZHA M, WANG C, LI C, JIANG Q C. Spheroidization of primary Mg_2Si in Al−20Mg_2Si−4.5Cu alloy modified with Ca and Sb during T6 heat treatment process [J]. Materials Science and Engineering A, 2017, 685: 31−38.

[55] LI K, ZHANG J, CHEN X, YIN Y, HE Y, ZHOU Z, GUAN R. Microstructure evolution of eutectic Si in Al−7Si binary alloy by heat treatment and its effect on enhancing thermal conductivity [J]. Journal of Materials Research and Technology, 2020, 9: 8780−8786. https://doi.org/10.1016/j.jmrt.2020.06.021.

[56] GAN Jun-qi, HUANG Yu-jian, WEN Cheng, DU Jun. Effect of Sr modification on microstructure and thermal conductivity of hypoeutectic Al−Si alloys [J]. Transactions of Nonferrous Metals Society of China, 2020, 30: 2879−2890. https://doi.org/10.1016/S1003-6326(20)65428-0.

[57] LUO G, ZHOU X, LI C B, HUANG Z H, DU J. A quantitative study on the interaction between silicon content and heat treatment on thermal conductivity of Al−Si binary alloys [J]. International Journal of Metalcasting, 2022, 16: 1585−1594. https://doi.org/10.1007/s40962-021-00706-4.

[58] AKSÖZ S, OCAK Y, MARAŞLI N, ÇADIRLI E, KAYA H, BÖYÜK U. Dependency of the thermal and electrical conductivity on the temperature and composition of Cu in the Al based Al−Cu alloys [J]. Experimental Thermal and Fluid Science, 2010, 34: 1507−1516. https://doi.org/10.1016/j.expthermflusci.2010.07.015.

[59] ZHANG C, DU Y, LIU S H, LIU Y L, SUNDMAN B. Thermal conductivity of Al−Cu−Mg−Si alloys: Experimental measurement and CALPHAD modeling [J]. Thermochimica Acta, 2016, 635: 8−16. https://doi.org/10.1016/j.tca.2016.04.019.

[60] RAVI K R, PILLAI R M, AMARANATHAN K R, PAI B C, CHAKRABORTY M. Fluidity of aluminum alloys and composites: A review [J]. Journal of Alloys and Compounds, 2008, 456: 201−210. https://doi.org/10.1016/j.jallcom.2007.02.038.

[61] SHIN J, KIM T, KIM D, KIM D, KIM K. Castability and mechanical properties of new 7xxx aluminum alloys for automotive chassis/body applications [J]. Journal of Alloys and Compounds, 2017, 698: 577−590. https://doi.org/10.1016/j.jallcom.2016.12.269.

[62] BAZHENOV V E, PETROVA A V, SANNIKOV A V, RIZHSKY A A, TITOV A Y, TSELOVALNIK Y V, OZHERELKOV D Y, PASHKOV I N, KOLTYGIN A V, BELOV V D. Relationship between critical solid fraction and dendrite coherency point in Al−Si alloys [J]. International Journal of Metalcasting, 2023, 17: 284−296. https://doi.org/10.1007/s40962-022-00772-2.

[63] CHEN R, XU Q Y, GUO H T, XIA Z Y, WU Q F, LIU B C. Correlation of solidification microstructure refining scale, Mg composition and heat treatment conditions with mechanical properties in Al−7Si−Mg cast aluminum alloys [J]. Materials Science and Engineering: A, 2017, 685: 391−402. https:// doi.org/10.1016/j.msea.2016.12.051.

[64] TAVITAS-MEDRANO F J, GRUZLESKI J E, SAMUEL F H, VALTIERRA S, DOTY H W. Effect of Mg and Sr-modification on the mechanical properties of 319-type aluminum cast alloys subjected to artificial aging [J]. Materials Science and Engineering: A, 2008, 480: 356−364. https://doi.org/10.1016/j.msea.2007.09.002.

[65] GUO F B, ZHU B H, JIN L B, WANG G J, YAN H W, LI Z H, ZHANG Y A, XIONG B Q. Microstructure and mechanical properties of 7A56 aluminum alloy after solution treatment [J]. Rare Metals, 2021, 40: 168−175. https://doi.org/10. 1007/s12598-017-0985-7.

[66] WANG E R, HUI X D, WANG S S, ZHAO Y F, CHEN G L. Improved mechanical properties in cast Al−Si alloys by combined alloying of Fe and Cu [J]. Materials Science and Engineering: A, 2010, 527: 7878−7884. https://doi.org/10.1016/j.msea.2010.08.058.

[67] JIANG H T, XING H, XU Z H, YANG B, LIANG E Q, ZHANG J, SUN B D. Effect of Zn content and Sc, Zr addition on microstructure and mechanical properties of Al−Zn−Mg−Cu alloys [J]. Journal of Alloys and Compounds, 2023, 947: 169246. https://doi.org/10.1016/j.jallcom.2023.169246.

[68] LADOS D A, APELIAN D, WANG L B. Solution treatment effects on microstructure and mechanical properties of Al−(1 to 13 pct)Si−Mg cast alloys [J]. Metallurgical and Materials Transactions B, 2011, 42: 171−180. https://doi.org/10.1007/s11663-010-9437-6.

[69] ZHU X M, LIU D, WANG J, CHEN C D, LI X X, WANG L, WANG M X. Effect of alloying elements on the short-range orders and atomic diffusion behavior of liquid Al−9Si cast alloys [J]. Materials, 2023, 16: 6768. https://doi.org/10.3390/ma16206768.

[70] OSÓRIO W R, PEIXOTO L C, GARCIA L R, GARCIA A. Corrosion behavior of hypoeutectic Al−Cu alloys in H_2SO_4 and NaCl solutions [J]. Acta Metallurgica Sinica (English Letters), 2009, 22: 241−246. https://doi.org/10.1016/S1006-7191(08)60095-2.

[71] VARGEL C. Corrosion of aluminium [M]. Amsterdam, The Netherlands: Elsevier, 2004.

[72] KAUFMAN J G, ROOY E L. Aluminum alloy castings: Properties, processes and applications [M]. Materials Park, USA: ASM International, 2004: 10.

高导热 Al−Zn−Ca 合金的铸造、力学和腐蚀性能

A. A. LYSKOVICH[1], V. E. BAZHENOV[1], I. I. BARANOV[1], V. A. BAUTIN[2], A. V. SANNIKOV[1], A. I. BAZLOV[3], E. I. TIAN[1], A. A. STEPASHKIN[4], A.V. KOLTYGIN[1], V. D. BELOV[1]

1. Casting Department, National University of Science and Technology “MISIS”, Moscow 119049, Russia;
2. Department of Metallurgy Steel, New Production Technologies and Protection of Metals, National University of Science and Technology “MISIS”, Moscow 119049, Russia;
3. Laboratory of Advanced Green Materials, National University of Science and Technology “MISIS”, Moscow 119049, Russia;
4. Center of Composite Materials, National University of Science and Technology “MISIS”, Moscow 119049, Russia

摘　要：大多数工业用铸造铝合金导热性能较低，无法满足电子设备中有效传热的需求。本研究旨在开发具有高导热性能的新型铝合金。研究了合金元素对纯铝导热性能的影响，并探讨了 Al−Zn−Ca−(Cu,Mg)合金的显微组织、导热性能、力学性能和耐腐蚀性能之间的关系。结果表明，在铸态下，合金组织由 α-Al 和含有 $(Al,Zn)_4Ca$ 相的共晶组成。经过固溶热处理后，$(Al,Zn)_4Ca$ 相发生球化，合金的导热性能提高，热导率达到纯铝的 75%以上。然而，热处理后的合金表现出较低的力学性能：抗拉屈服强度低于 60 MPa，极限抗拉强度低于 160 MPa，断裂伸长率大于 15%。合金表现出良好的流动性及较低的热裂敏感性。除含铜合金外，其余合金的腐蚀速率均较低，约为 0.02 mm/a。

关键词：铝合金；热导率；相组成；　流动性；热裂敏感性；腐蚀速率

(Edited by Xiang-qun LI)